THE ASTROPHYSICAL JOURNAL SUPPLEMENT SERIES, 61:219–248, 1986 June

DYNAMICS OF AN AFFINE STAR MODEL IN A BLACK HOLE TIDAL FIELD

JEAN-PIERRE LUMINET AND BRANDON CARTER
Groupe d'Astrophysique Relativiste, Observatoire de Paris, Meudon, France
Received 1985 May 13; accepted 1985 December 2

ABSTRACT

It has recently been shown that the tidal disruption of a star moving in a deeply plunging orbit in the field of a large black hole such as may occur in an active galactic nucleus can most conveniently be studied in a first approximation using a simple affine star model. Preliminary investigations have shown that the (positive) nuclear energy released during a short-lived phase of compression to a highly flattened pancake configuration can more than counterbalance the (negative) self-binding energy of the original stellar configuration, so that instead of ending up weakly bound to the central black hole (as had been supposed in earlier studies based on a less realistic incompressible model) the gas may ultimately be blown out with net positive energy.

The present work contains explicit results of numerical integration of the dynamical equations of motion of the affine star model in various cases that have not been examined in detail before, concentrating on the regime prior to the release of dynamically significant nuclear energy, where the model can be expected to be most reliable. In addition to studies aimed at improved realism in the treatment of medium-mass and higher mass stars on the basis of the natural affine analog of Eddington's standard model (using a simple treatment of the separate contributions of gas and radiation pressure), the present work also includes studies of the incompressible limit, aimed at completing the classical work on this subject, and also studies of the effect of (artificially high) viscous dissipation, aimed at comparison with the first crude hydrodynamic investigations, in which artificial dissipative effects are important.

Subject headings: black holes — active galactic nuclei

I. INTRODUCTION

It is widely recognized that gravitational accretion of gas onto a black hole (or more generally a compact body) is one of the most potentially efficient processes of energy release, and therefore likely to be relevant to many highly energetic astrophysical phenomena, particularly in active galactic nuclei. In addition to the accretion of free gas (whose origin may pose a problem), the interaction between a black hole and a *whole* (bound) star probably plays a key role in active galactic nuclei, as was pointed by Wheeler (1971) and Hills (1975): in the neighborhood of a black hole with mass less than the critical value originally calculated (in another context) by Michell (1784), a star can be tidally torn apart *outside* the horizon and thus liberate at least some fraction of its gas available for further accretion onto the black hole.

Most of the original gas production scenarios involving tidal breakup of stars by a giant black hole (Frank and Rees 1976; Young, Shields, and Wheeler 1977) were based on the extrapolation of the strictly homogeneous, *incompressible* fluid model. It was generally assumed that any star penetrating within the Roche tidal radius of a black hole, given in order of magnitude in terms of the mass M of the hole and the (uniform) density of the star, ρ_*, by

$$R_{\mathrm{R}} \approx (M/\rho_*)^{1/3}, \tag{1.1}$$

would be sufficiently excited by the external tidal field to undergo uncontrolled oscillations, leading ultimately to complete disruption into miscellaneous debris such as diffuse clouds, filaments, doughnuts, and so on, that remain weakly bound to the black hole (Hills 1978; Frank 1979; Gurzadyan and Ozernoy 1980). Such a relatively quiescent scenario for the breakup of a star is rather in contrast with the radical violence of the astrophysical context in which the question arose, namely, a strong gravitational field crushing the incoming matter so as to produce huge quantities of outcoming radiation.

Actually, as recently pointed out by the present authors (Carter and Luminet 1982, hereafter CL82), this unrealistically placid picture resulted from the assumption of incompressibility, which prevented the external tidal field from achieving one of its most important tendencies, namely, to produce compression along two of its three principal directions. In fact, in a more realistic description in which the star is not artificially constrained to keep a constant volume, the dominant tendency to compression can have a very considerable crushing effect in the plane of the orbit in case of *deep penetration* of the body within the Roche radius (essentially because the direction orthogonal to the orbital plane is a *fixed* compressive principal direction of the tidal field), which can occur provided that the Schwarzschild radius is sufficiently small compared with the Roche radius (in particular in the black hole mass range 10^5–10^7 $M_\odot$ for solar-type stars). Therefore, although the final tendency remains the dispersal of the stellar gas, the disruption is preceded by a short-lived phase of high compression to a flattened "pancake" configuration, in which the density and the temperature may rise enough to trigger explosive nucleosynthesis in the core of the star. The resulting energy release may be sufficient for the gas to become unbound so that much of it escapes from the black hole gravitational field, with the consequence that the working of the entire accretion process should be substantially modified.

While the simplifying assumption of incompressibility is well justified in a planetary context (to which the studies of tides were originally devoted), it is thus utterly inappropriate for ordinary stars moving in a strong, rapidly varying tidal field. It is clear that the full compressible problem is much more complex than the incompressible one, since, when the fluid is not homogeneous, the self-gravitational potential within it will no longer be a quadratic function of the internal coordinates, and thus the fluid cannot keep an ellipsoidal shape. Therefore, the search for detailed solutions must be based on hydrodynamical treatment. Another difficulty then appears, due to purely numerical limitations. For instance, Nolthenius and Katz (1983) have recently performed three-dimensional simulations of the passage of a polytropic star near a massive black hole, finding as expected that the star is ultimately disrupted for sufficiently small periastron distances (in the sense that its central density goes down to zero after the passage). However, as they themselves recognized, the spatial resolution of their calculations was so poor that no description of the geometrical structure of the deformed star could be given reliably: since the gross final tendency was the disruption of the star (as expected from the extrapolation of the incompressible model), they drew the unsound conclusion that a rapidly varying potential (as occurs for stars moving along eccentric orbits) produces qualitatively the same effects as a static potential (in which the assumption of incompressibility is much better justified). It was in order to obtain estimates more realistic than those that can be obtained from a hydrodynamical treatment with inadequate resolution that the present authors were led to introduce the *affine* treatment (Carter and Luminet 1983, 1985, hereafter CL83, CL85) that is used here. A satisfactory hydrodynamical treatment should nevertheless become feasible in the near future because of the increased availability of sufficiently powerful computing facilities.

The general basic properties of the simplified affine star model (in which the density contours are restrained so as to keep a homologous ellipsoidal shape) are described in some detail in CL85. In our previous application of this model (CL83), we considered the case of small main-sequence stars in orbits with a moderate value $5 < \beta < 15$ for the factor β of penetration within the Roche radius, for which a polytropic model with $\gamma = 5/3$ is appropriate, and it was confirmed that for a stellar Population I type chemical composition, the energy release resulting from proton capture by medium-weight elements (C, N, O) could more than outweigh the loss of the gravitational binding energy. A subsequent application of the same $\gamma = 5/3$ polytropic model to the case of more deeply plunging orbits, say with $15 < \beta < 30$, by Pichon (1985) and Luminet and Pichon (1986) showed that additional energy release resulting from triple-α and subsequent helium-burning reactions in a hydrogen-rich medium might be of at least the same order of magnitude, even though it could never reach the even higher magnitudes whose possibility was considered in our original (CL82) speculation. (It must be emphasized that for such very high values of the penetration factor, the validity of the affine treatment can no longer be taken for granted, so that the results must be considered merely provisional, subject to confirmation by a more accurate hydrodynamical analysis.) In the most recently published application of the affine model, still restricted to the $\gamma = 5/3$ polytropic case, Luminet and Marck (1985) have investigated the general-relativistic effects that will be important in the case of very massive black holes for which the Schwarzschild radius is comparable to the minimum radius of the plunging orbit under consideration, the most noteworthy result being the discovery that a second pancake compression phase (and hence the possibility of a second important nuclear energy release) is likely to occur a few minutes after the first.

Our purpose in the present work is to give a more detailed description of the behavior of the affine model in the regimes for which it can be expected to be most reliable, before the onset of any dynamically significant thermonuclear energy release. As well as provisionally leaving aside such (ultimately important) internal energy generation effects, the present study takes no account of the general relativistic effects that will in any case be significant only for a central black hole close to the Michell-Laplace-Hills limiting mass (in the range 10^7–10^8 $M_\odot$ for main-sequence stars), above which the Schwarzschild radius exceeds the Roche disruption radius.

Despite the limitations just referred to, the present work goes beyond our previous applications of the affine model in several respects, including notably the use of equations of state more general than that of a simple $\gamma = 5/3$ polytrope, inclusion of viscosity, and investigation of the low penetration limit below which disruption does not take place.

After a recapitulation of the basic properties of the affine model in § II, the first new results are presented in § III, which deals with the incompressible limiting case, in order to relate the present sequence of investigations (motivated by stellar disruption problems) to the classic sequence of investigations (motivated by planetary disruption problems, for which an incompressible treatment is a not unreasonable first approximation) that was initiated by Roche (1847). Our present results complete much earlier work on the subject by providing the first reasonably precise numerical solution of the problem of calculating the critical radius for dynamical disruption of an incompressible fluid model in a parabolic orbit.

After this more mathematically than physically motivated digression, we proceed in § IV to discuss more general compressible models that will be relevant in the stellar case. The $\gamma = 5/3$ polytropic model used in our earlier investigations can be expected to be adequate for the treatment of small main-sequence stars subject to moderate compression factors, but for medium- and high-mass main-sequence stars, for which radiation pressure will (at least initially) be dominant, it will be more adequate to use a *standard model* obtained as a natural adaptation of the Eddington standard model that played an important role in the early development of stellar equilibrium theory.

The actual application of such compressible models to the parabolic disruption scenario is described in § V. For calculation of the critical radius for disruption, the distinction between the simple $\gamma = 5/3$ polytropic model and the more elaborate standard model is not very important, but for calculation of the maximum densities obtained during the compressed pancake phase the distinction is highly significant.

The purpose of the final section is to examine the effect of modifying the adiabatic treatment by inclusion of viscosity. It is shown that, with a suitably chosen artificial viscosity, the affine model can be used to simulate the behavior of the hydrodynamical star model recently employed for studying the parabolic stellar disruption process by Bicknell and Gingold (1983). On the basis of their numerical work, these authors have suggested that the orders of magnitude of the maximum density (although not of the temperature) in the pancake configuration predicted by the present authors (CL82, CL83) should be greatly reduced because of the effect of entropy generation by shocks resulting from deviations from affine behavior. This would not significantly affect the proton capture process on C,N,O elements (CL83), but, as emphasized by Bicknell and Gingold (1983), it would greatly reduce the energy release to be expected from the more density-sensitive triple-α reaction. The demonstration here that the numerical results of the Bicknell and Gingold calculation can be simulated by the affine model with artificial viscosity should not be interpreted as confirmation of their conclusion: their spatial resolution was too low for adequate treatment of shocks, their entropy production being attributable to the artificial viscosity needed for stability of the numerical scheme. Although it is to be expected that shock formation will ultimately become important, our own conjecture, supported by heuristic considerations put forward by S. Bonazzola (1985, private communication) on the basis of analogies with spherical collapse situations, is that shock dissipation will not become important until shortly *after* the phase of maximum density. A definitive conclusion of this debate must await the availability of a sufficiently high resolution hydrodynamical treatment.

II. THE AFFINE EQUATIONS OF MOTION

Let us consider an infinitesimal material element of the star model located at coordinates x_i $(i=1,2,3)$ in an ordinary inertial Cartesian system of reference, whose origin may be identified with the position of the black hole when the mass M of the latter is much greater than the mass M_* of the star. One can use the decomposition

$$x_i = X_i + r_i, \tag{2.1}$$

where the X_i are the inertial coordinates of the center of mass of the star and the r_i are coordinates of the material element relative to the center of mass of the star in a parallel-propagated frame.

The affine star model is based on the assumption that the relative position vector $\boldsymbol{r}$ is specified by a linear relation of the form

$$r_i = q_{ia}\hat{r}_a \qquad (i, a = 1,2,3;\ \text{repeated indices are summed}), \tag{2.2}$$

where $\hat{\boldsymbol{r}}$ is the position vector of the same element in a reference state (e.g., exact spherical equilibrium configuration), and the 3×3 matrix $\mathbf{q}$ is spatially uniform in the sense that its component values depend only on the time t but are independent of the element under consideration.

Under the influence of the affine transformation (2.2), the initial spherical configuration of radius $\hat{r} = (\hat{r}_a\hat{r}_a)^{1/2}$ (which can without loss of generality be set equal to unity) is transformed into the ellipsoid of locus

$$S_{ij}^{-1} r_i r_j = 1, \tag{2.3}$$

where $\mathbf{S}^{-1}$ is the inverse of the configuration matrix $\mathbf{S}$ defined by

$$S_{ij} = q_{ia} q_{ja}, \tag{2.4}$$

so that the eigenvalues of $\mathbf{S}$ are directly interpretable as the squares of the magnitudes of the principal axes of the ellipsoid. The main purpose of the affine relation (2.2) is to allow compressibility of the stellar material, since the mass density $\hat{\rho}$ associated with a given material element in the reference state is transformed into

$$\rho = |\mathbf{q}|^{-1}\hat{\rho}, \tag{2.5}$$

where $|\mathbf{q}|$ is the determinant of the deformation matrix $\mathbf{q}$, which can obviously be interpreted as a volume factor.

The affine model is the simplest and most natural generalization of the incompressible fluid model (in which ellipsoidal configurations are *exact* solutions). Its basic equations of motion can be written in the form (CL85)

$$\mathcal{M}_*\ddot{q}_{ia} = \mathcal{M}_* C_{ij} q_{ja} + \Pi q_{ai}^{-1} + \Omega_{ij} q_{aj}^{-1} - \Sigma_{ij} q_{aj}^{-1}, \tag{2.6}$$

where a dot denotes time differentiation and where the constant factor

$$\mathscr{M}_* = \frac{1}{3}\int \hat{r}_a \hat{r}_a \, dM \tag{2.7}$$

is the scalar quadrupole moment of the star model in the spherical reference state.

The first three terms on the right-hand side of equation (2.6) represent the nondissipative force contributions due respectively to the *tidal* (external), the *pressure* (internal), and the *self-gravitational* (internal) force fields, while the last term corresponds to an eventual *dissipative* internal force contribution that can arise when viscosity of the stellar material is taken into account and whose application will be reported in § VI.

For our present purpose let us just recall the explicit expressions of the various terms appearing in equation (2.6) needed to carry on numerical integration. $C_{ij} = C_{ij}(\boldsymbol{X})$ are the component values, at the center of mass of the star, of the trace-free symmetric tidal matrix **C**, defined in terms of the external gravitational potential Φ_E generated by the black hole, by

$$C_{ij} = \frac{\partial^2 \Phi_E}{\partial x_i \, \partial x_j}, \tag{2.8}$$

with

$$\Phi_E(\boldsymbol{X}) = \frac{-GM}{(X_i X_i)^{1/2}}. \tag{2.9}$$

Introducing suitably chosen coordinates

$$X = X_1, \qquad Y = X_2, \qquad Z = X_3, \qquad R^2 = X^2 + Y^2 + Z^2 \tag{2.10}$$

such that the space trajectory of the center of mass of the star model is confined within the plane $Z = 0$, one deduces the following explicit form of the tidal matrix:

$$C_{ij}(\boldsymbol{X}) = -\frac{GM}{R^3}\begin{pmatrix} 1-3X^2/R^2 & -3XY & 0 \\ -3XY & 1-3Y^2/R^2 & 0 \\ 0 & 0 & 1 \end{pmatrix}. \tag{2.11}$$

The time evolution of the tidal matrix obviously depends on the orbital law of motion of the star's center of mass. When we assume that the dimensions of the star model are small compared with the characteristic length scale of the external field, the deviation tensor (defined as the spatial derivative of the tidal tensor) can be neglected, so that the motion of the center of mass of the star reduces to the free-fall motion of a particle with mass M_* in the gravitational potential (2.9). Moreover, in any plausible situation expected in a galactic nucleus, the part of the orbit within the region of strong gravitational tidal forces (i.e., $R \lesssim R_{\mathrm{R}}$) can be approximated very well as a parabola of locus

$$X = \frac{Y^2}{4R_p} - R_p, \qquad Z = 0, \qquad R = \frac{Y^2}{4R_p} + R_p, \tag{2.12}$$

with time motion given by

$$t = \frac{Y}{(2GMR_p)^{1/2}}\left(\frac{Y^2}{12R_p} + R_p\right). \tag{2.13}$$

The periastron distance R_p is related to the orbital angular momentum per unit mass, J, by

$$J = (2GMR_p)^{1/2}, \tag{2.14}$$

and the origin of time has been taken at the instant of passage at periastron.

The quantity Π appearing in the pressure force contribution is defined as the volume integral of the local pressure P, i.e.,

$$\Pi = \int \frac{P}{\rho} \, dM. \tag{2.15}$$

Analogously introducing the internal gas compression energy U as the volume integral of the local energy density $\mathscr{E}$ according to

$$U=\int \frac{\mathscr{E}}{\rho}\, dM, \tag{2.16}$$

one can show (CL83, CL85) that the pressure integral Π is directly related to U by

$$\Pi=-|\mathbf{q}|\frac{\partial U}{\partial|\mathbf{q}|}. \tag{2.17}$$

The explicit dependence of the global quantities Π and U in terms of the deformation matrix $\mathbf{q}$ will be given by an equation of state of the stellar material, to be specified in § IV.

The term Ω_{ij} is the self-gravitational energy tensor, which can be shown to be given in terms of the configuration matrix $\mathbf{S}$ by a relation involving elliptic integrals (see Appendix A), of the form

$$\Omega_{ij}=\tfrac{1}{2}|\mathbf{S}|^{-1/2}A_{ik}S_{jk}\Omega_*, \tag{2.18}$$

where

$$A_{ij}=|\mathbf{S}|^{1/2}\int_0^\infty du\frac{(\mathbf{S}+u\mathbf{1})_{ij}^{-1}}{|\mathbf{S}+u\mathbf{1}|^{1/2}} \tag{2.19}$$

and Ω_* is the self-gravitational energy value in the spherical reference state. From the usual virial theorem, the latter is related to the reference state value Π_* of the pressure integral by

$$\Omega_*=-\Pi_*/3. \tag{2.20}$$

The last term in equation (2.6) Σ_{ij} is the dissipative internal force moment defined as the volume integral of the dissipative stress tensor z_{ij} according to

$$\Sigma_{ij}=\int\frac{z_{ij}}{\rho}\, dM. \tag{2.21}$$

To conclude this section, let us remark that the equations of motion for ellipsoidal configurations are usually written in the principal axis frame (see, e.g., Chandrasekhar 1969). Since tidal perturbations induce generally oscillations, angular momentum, and internal motions, the ellipsoidal configuration at any time t can be completely described by the instantaneous values of the magnitudes of the three principal axes $a_i(t)$, of the three components $w_i(t)$ of the angular velocity vector (rotation rate of the principal axis frame relative to the inertial frame), and of the three components $\zeta_i(t)$ of the shear vector (rotation rate of the fluid relative to the principal frame). Transformation formulae between the nine center-of-mass frame quantities q_{ia} and the nine principal axis frame quantities a_i, w_i, ζ_i are straightforward (see Appendix B).

III. TIDAL DESTRUCTION OF HOMOGENEOUS INCOMPRESSIBLE BODIES

As already remarked in CL83, the incompressible fluid model can be considered as a degenerate case of the affine model, in the sense that when a body is constrained to keep a constant volume, the corresponding equations of motion are obtainable from the affine equations (2.6) by replacing the internal energy term U by the product of the determinant $|\mathbf{q}|$ with a Lagrange multiplier, the latter being directly interpretable as the central pressure P_c. The equations of motion then become

$$\ddot{q}_{ia}=C_{ij}q_{ja}-\frac{3}{2}\frac{\Pi_*}{\mathscr{M}_*}\Omega_{ij}q_{aj}^{-1}+P_c(t)|\mathbf{q}|q_{ai}^{-1}, \tag{3.1a}$$

$$|\mathbf{q}|=1. \tag{3.1b}$$

Since for the homogeneous sphere the pressure integral Π_* and the quadrupolar mass $\mathscr{M}_*$ are respectively given in terms of the mass M_* and the radius R_* by

$$\Pi_*=\frac{1}{5}\frac{GM_*^2}{R_*}, \qquad \mathscr{M}_*=\frac{3}{5}M_*R_*^2, \tag{3.2}$$

one deduces

$$\frac{\Pi_*}{\mathscr{M}_*} = \frac{1}{3}\frac{GM_*}{R_*} = \frac{4}{9}\pi G\rho_*, \tag{3.3}$$

where ρ_* is the (uniform) density of the body (which we shall refer to in the incompressible case as the satellite; it would evidently be inappropriate to describe it as a star).

A lot of work has been done on the study of the figures of equilibrium of homogeneous bodies moving in a *stationary* tidal field along synchronized circular orbits, i.e., with angular velocity of orbit equal to that of the principal axes (ellipsoidal solutions of the stationary problem are obviously obtainable from eqs. [3.1] by setting the derivative term equal to zero). It is well known since Roche (1847) that the rigid (i.e., without internal motions) equilibrium states can exist only if the radius of circular orbit is greater than a critical limit depending on the ratio of masses of the two bodies. In the case of an infinitesimal satellite (i.e., $M_* \ll M$), Roche derived the famous expression

$$R_{\rm R} = 1.523(M/\rho_*)^{1/3} = 2.455(M/M_*)^{1/3} R_*. \tag{3.4}$$

More than one century later, by simple application of the classical works of Dirichlet, Dedekind, and Riemann, Aizenman (1968) generalized the rigid Roche ellipsoids to include the case of differentially rotating bodies with uniform vorticity. The corresponding *Roche-Riemann limit* is given by

$$R_{\rm RR} = 1.512(M/\rho_*)^{1/3}. \tag{3.5}$$

Much of the work by the classical authors in this field has been devoted to the question of stability of the equilibrium configurations in the neighborhood of the Roche limit. Earlier workers such as Darwin (1911) would seem to have supposed that instability first sets in along a sequence of increasing ellipticity at exactly the Roche limit point, where the angular velocity of the configuration reaches a maximum, but Chandrasekhar (1963) showed that the Coriolis effect allows the configurations to remain stable a little way beyond this point.

The exact limit at which disruption of an incompressible model will occur in a *dynamic* scenario involving a plunging orbit was not seriously investigated until more recently, when better numerical computation facilities became available. The case of closed eccentric orbits has been treated numerically by Nduka (1971), who affirmed that if the satellite penetrates inside the stationary Roche limit, it will be disrupted in the sense that its figure tends rapidly to a disklike configuration (flattening toward the orbital plane and extension within the orbital plane). Unfortunately, Nduka's discussion of results was very brief and incoherent (for example, he gave no characteristic time scale of flattening, and he stated that one axis tends to zero while the other two remain finite, which is of course incompatible with volume constancy).

We present here a new numerical integration of the equations of motion (3.1) for homogeneous bodies moving along parabolic orbits within a wide range of periastron distances. The *effective* Roche limit, i.e., the critical distance within which any penetrating body bifurcates to a regime where its central pressure falls to zero, is found to occur in the range (within the best precision of the present calculation)

$$1.49\left(\frac{M}{\rho_*}\right)^{1/3} \le R_{\rm inc} \le 1.52\left(\frac{M}{\rho_*}\right)^{1/3}, \tag{3.6}$$

i.e., very close to the stationary Roche-Riemann limit (3.5). When the periastron distance R_p is slightly greater than this limit (Figs. 1–3), the tidal forces are not sufficient to destroy the satellite, but they induce rotation, vorticity, and oscillations of the axes around mean values (depending on R_p) characteristic of a *Riemann type S ellipsoid* (Riemann ellipsoids are stationary figures of equilibrium of isolated rotating bodies with internal motions; "type S" means that the directions of the angular velocity vector $\boldsymbol{w}$ and of the shear vector $\boldsymbol{\zeta}$ are parallel and coincide with the least principal axis [see, e.g., Chandrasekhar 1969, chap. 7). Moreover, since it was assumed that the satellite is initially (asymptotically far from the source) a nonrotating sphere, and recalling the property that the fluid circulation is conserved along the motion of a nonviscous body in an external tidal field, we find that the "output" Riemann configuration is also *irrotational*, i.e., although the fluid rotates relatively to the principal axis frame, its vorticity as evaluated in the center-of-mass frame remains zero. These results illustrate clearly a new interesting type of *bifurcation* induced by a weak tidal perturbation, the position on the final Riemann sequence depending only on the periastron distance R_p.

Turning now to the still more interesting case where the satellite is disrupted, i.e., when one at least of its principal axes increases to infinity, we have discovered two different regimes of disruption, associated respectively with final cigar-like or disklike shapes. More precisely, when

$$0.16 R_{\rm inc} \le R_p \le R_{\rm inc}, \tag{3.7}$$

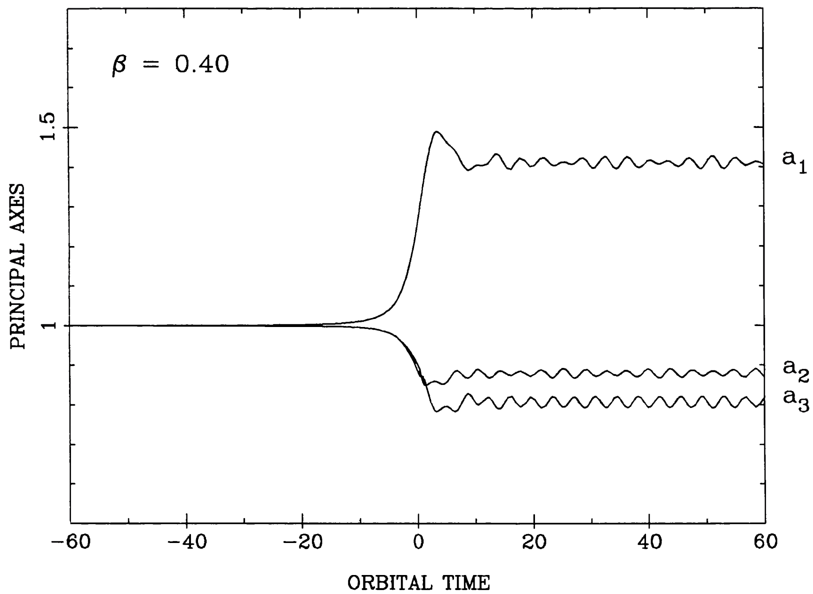

FIG. 1a

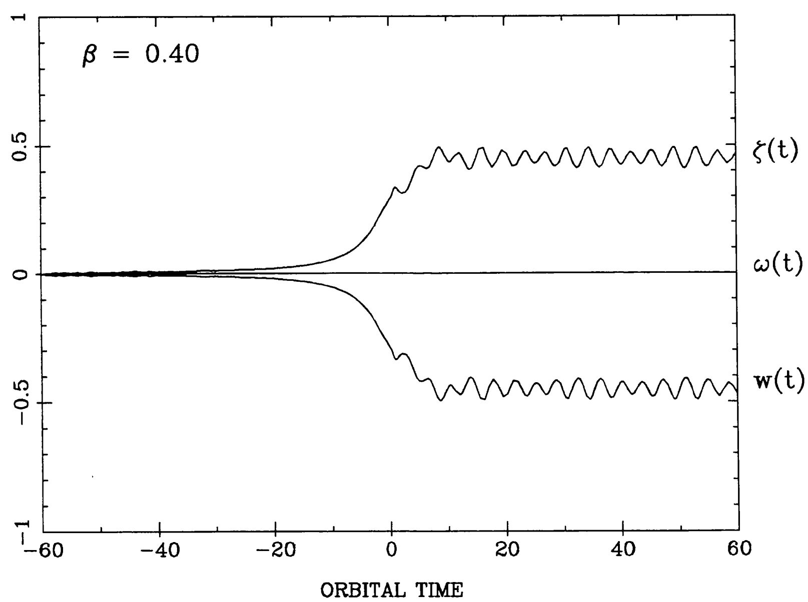

FIG. 1b

FIG. 1.—Time evolution of the incompressible model along a parabolic orbit with penetration factor $\beta = 0.40$ (where β is defined as the ratio between the characteristic Roche radius $(M/\rho_*)^{1/3}$ and the periastron distance R_p). The orbital time is in units of the stellar dynamical time $\tau_* = (\pi G \rho_*)^{-1/2}$. Periastron is at $t = 0$; the star enters the Roche radius at $t \approx -1$ and leaves it at $t \approx +1$. (a) Time variations of the principal axes. The primary is not disrupted but under the effect of the tidal perturbation bifurcates toward an average Riemann ellipsoidal configuration with angular momentum and vorticity. (b) The angular velocity vector $\boldsymbol{w}$, the shear vector $\boldsymbol{\zeta}$, and the rotation vector $\boldsymbol{\omega}$ (see Appendix B). Since the initial spherical configuration is irrotational, $\boldsymbol{\omega}(t) \equiv \boldsymbol{w}(t) + \boldsymbol{\zeta}(t) = 0$ along the motion.

the satellite elongates along the "radial" principal direction (say axis a_1) while it shrinks along the two other directions (say a_2, a_3). This is the *cigar regime* (Figs. 4 and 5). Axes a_2, a_3 oscillate around mean monotonically decreasing values very close to each other, and the average amplitude of oscillations increases rapidly with decreasing R_p.

The transition toward the *disk regime* occurs for

$$R_p \leq 0.16 R_{\rm inc}, \tag{3.8}$$

i.e., at least for a penetration by a factor of 6 within the effective Roche limit. As predicted by Nduka (1971), the satellite stretches to infinity within the orbital plane, while it flattens along the orthogonal direction (Fig. 6).

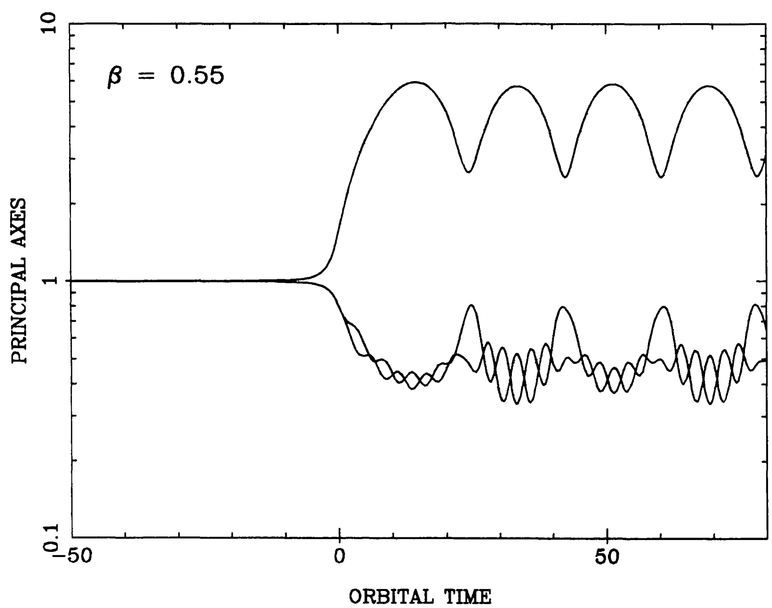

FIG. 2.—Time variations of the principal axes for the incompressible model with $\beta = 0.55$

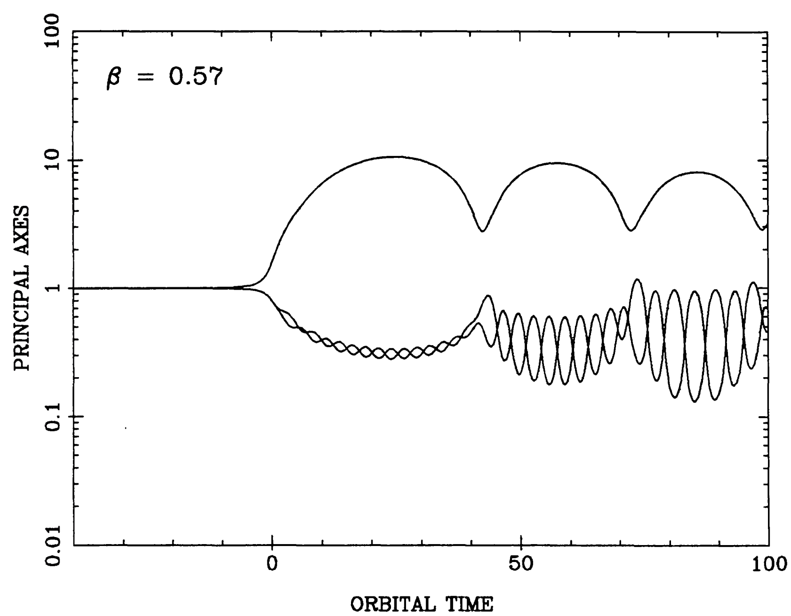

FIG. 3.—Time variations of the principal axes for the incompressible model with $\beta = 0.57$. The periastron distance is a little bit greater than the effective disruption limit (3.6), so that the primary is on the verge of being broken.

As we shall see in the next sections, dropping the assumption of incompressibility leads to still more spectacular deformations.

IV. EQUATIONS OF STATE

a) *Adiabatic versus Nonadiabatic Variations*

In order to complete the specification of the general affine star model, one has still to determine the explicit form of the internal gas pressure contribution Π given the equation of state of the stellar material, i.e., given the energy density $\mathscr{E}$ as a function of local thermodynamic conditions. In view of its conservation property, it is judicious to introduce a natural adiabatic invariant, namely, the entropy per unit mass,

$$\sigma = s/\rho, \tag{4.1}$$

where s is the entropy density and ρ is the mass density.

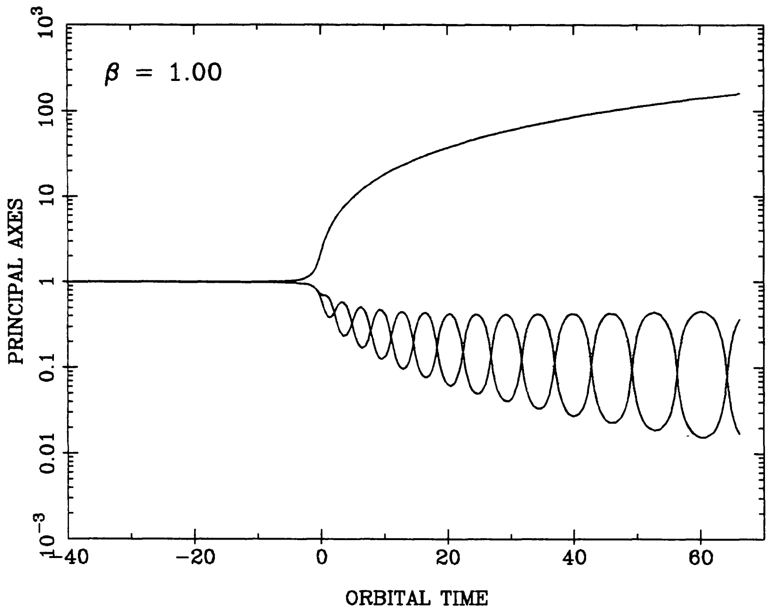

FIG. 4a

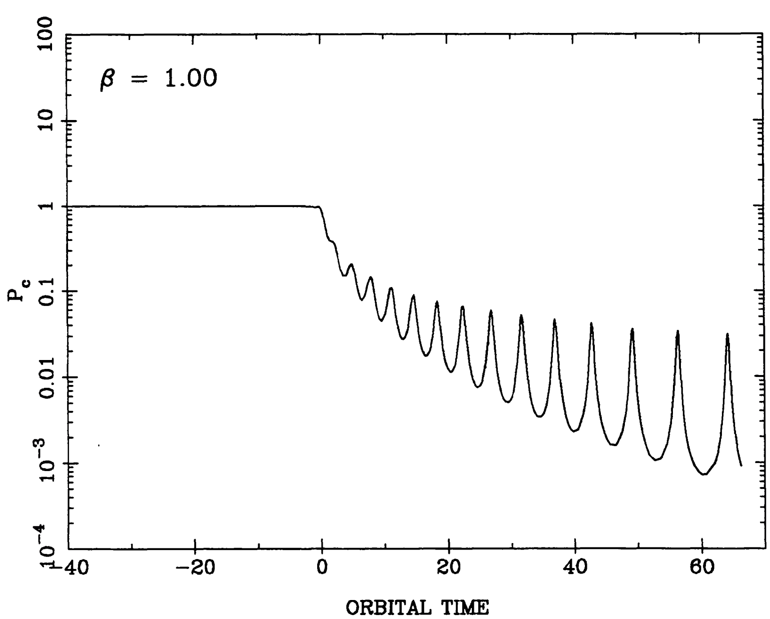

FIG. 4b

FIG. 4.—Incompressible model with $\beta = 1.00$. (a) Principal axes. (b) Central pressure P_c (in units of the equilibrium central pressure). The primary is now disrupted when it leaves the Roche radius, evolving toward a "cigar-like" configuration. (c–d) Trajectories in the $(a_2/a_1, a_3/a_1)$-plane of the incompressible model; in (c) we have represented by a dot the point where the periastron distance is reached. The departure from spheroidal configuration occurs somewhat later, as depicted in (d), which is an enlargement of the dashed square of (c).

Neglecting additional parameters such as chemical composition, the energy density $\mathscr{E}$ is generally a function of ρ and σ:

$$\mathscr{E} = \mathscr{E}(\rho, \sigma). \tag{4.2}$$

In a general thermodynamical transformation, the local gas pressure P and temperature T are determined by the infinitesimal variation law,

$$d\left(\frac{\mathscr{E}}{\rho}\right) = \frac{P}{\rho}\frac{d\rho}{\rho} + T d\sigma. \tag{4.3}$$

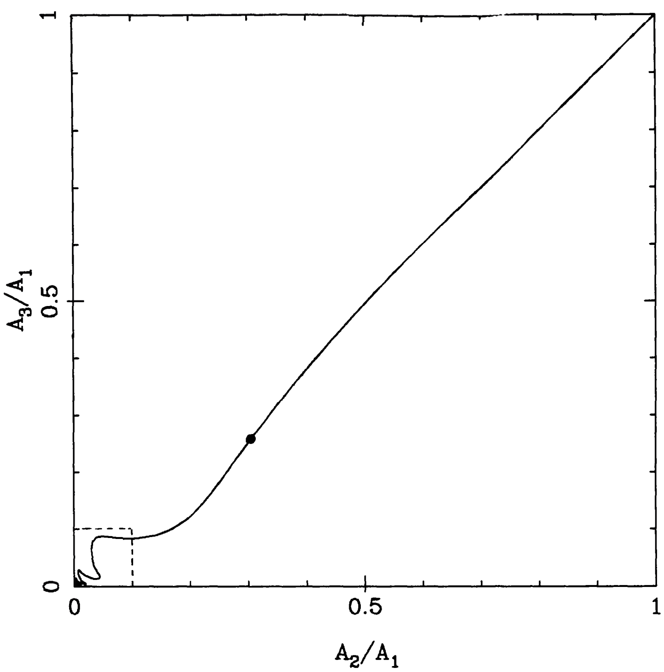

FIG. 4*c*

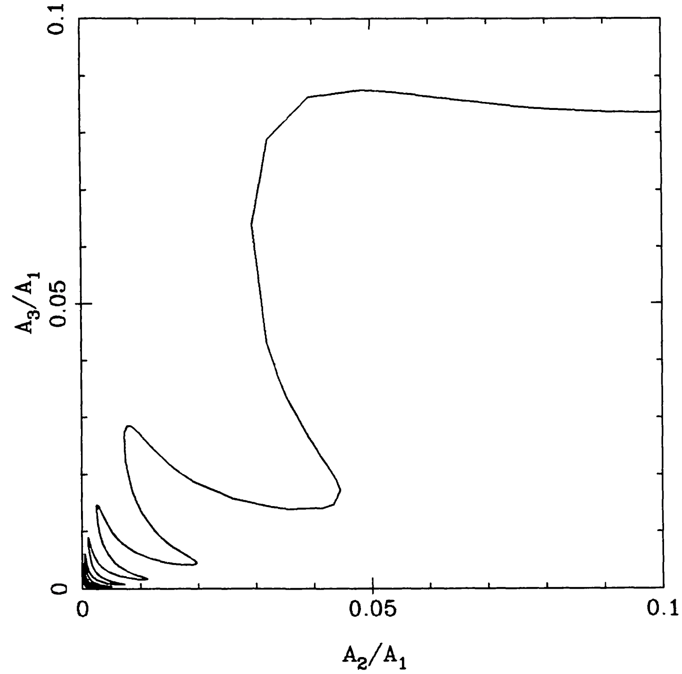

FIG. 4*d*

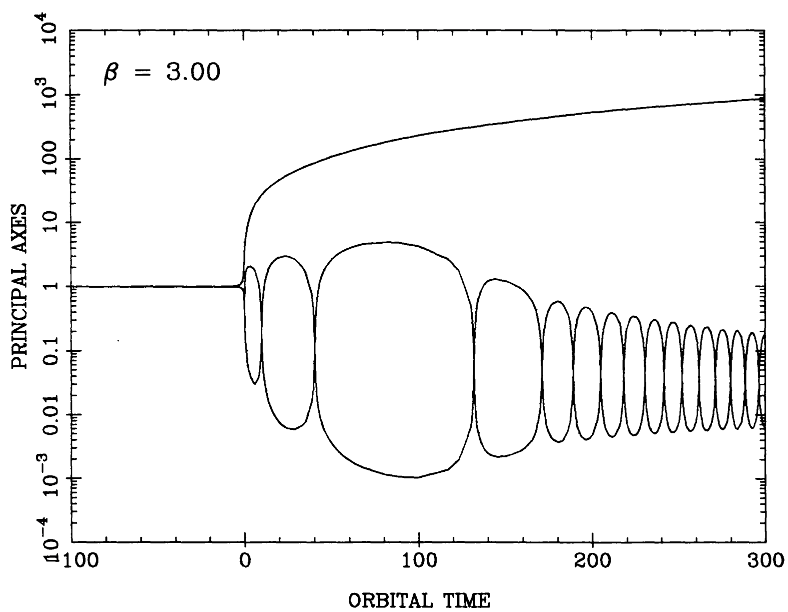

FIG. 5.—Incompressible model with $\beta = 3.00$. The transition to the disklike regime of disruption is not far, so that the oscillations of the a_2, a_3 least axes have very large amplitudes.

Considering the total gas compression energy U as a *time-dependent* function of the density distribution, one obtains from equations (2.5) and (4.3)

$$dU = -\Pi \frac{d|\mathbf{q}|}{|\mathbf{q}|} + \frac{\partial U}{\partial t} dt, \tag{4.4}$$

where

$$\frac{\partial U}{\partial t} = \int T \dot{\sigma} \, dM \tag{4.5}$$

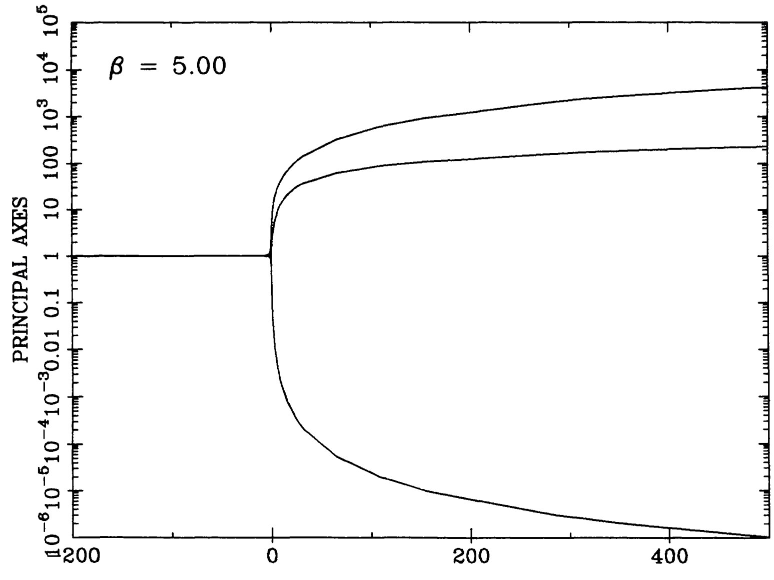

FIG. 6a

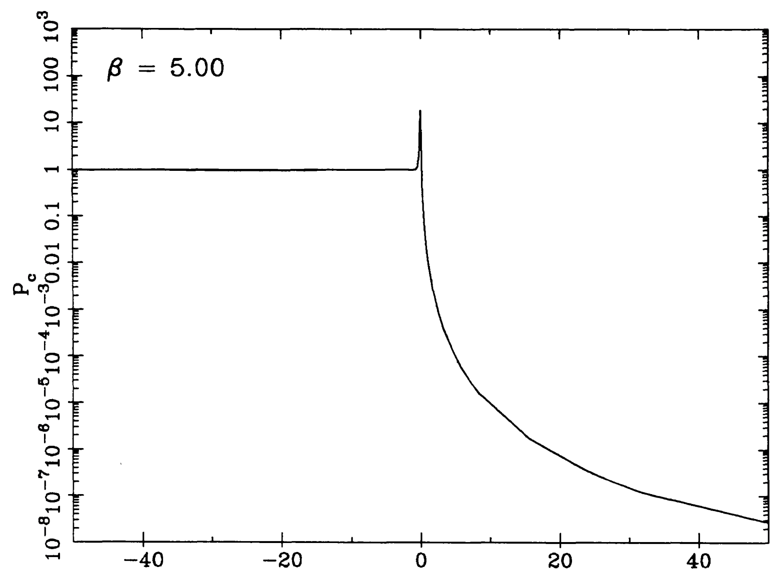

FIG. 6b

FIG. 6.—Incompressible model with $\beta = 5.00$. (a) Principal axes. The asymptotic output configuration is a disk infinitely flattened in the orbital plane. (b) The central pressure initially increases *in the same time* as the tidal forces, in order to preserve the volume-invariance constraint. As a consequence, the production of a short "pancake" effect is forbidden by the assumption of incompressibility.

represents the nonadiabatic contribution to gas energy variations. This latter can generally be written as

$$\frac{\partial U}{\partial t} = \dot{Q}_N - \dot{Q}_V, \tag{4.6}$$

where $\dot{Q}_N$ denotes the total power *injected* by nuclear sources and $\dot{Q}_V$ denotes the power *dissipated* by viscous stresses.

b) *The Polytropic Affine Star Model*

In the simplest applications of the affine star model (such as those already discussed in CL83, CL85) it will be sufficient to use a *polytropic* perfect gas equation of state of the form

$$\mathscr{E} = \psi(\sigma)\rho^{\gamma}, \tag{4.7}$$

where γ is the ratio of specific heats (considered as constant and uniform over the volume of the star model), and ψ is a factor that depends only on the entropy per unit mass and thus remains constant in adiabatic variations. From equation (4.3) the gas pressure and temperature are given by

$$P = (\gamma - 1)\psi\rho^{\gamma}, \tag{4.8}$$

$$T = \frac{d\psi}{d\sigma}\rho^{\gamma-1}, \tag{4.9}$$

while the gas energy integral U and the pressure integral Π as defined by equations (2.15) and (2.16) take the very simple form

$$U = \mathscr{M}_{*}\Psi|\mathbf{q}|^{1-\gamma}, \tag{4.10}$$

$$\Pi = (\gamma - 1)U. \tag{4.11}$$

Here the integral factor Ψ is a function only of the entropy distribution:

$$\Psi = \frac{1}{\mathscr{M}_{*}}\int \psi\hat{\rho}^{\gamma-1}\,dM. \tag{4.12}$$

In *adiabatic* variations, Ψ remains constant, equal to its spherical equilibrium reference state value

$$\Psi_{*} = \frac{\Pi_{*}}{(\gamma-1)\mathscr{M}_{*}}, \tag{4.13}$$

while the temperature is merely given in terms of the equilibrium value T_{*} by

$$T = T_{*}|\mathbf{q}|^{1-\gamma}. \tag{4.14}$$

In *nonadiabatic* variations, the entropy integral Ψ is a solution of the differential equation

$$\dot{\Psi} = \frac{|\mathbf{q}|^{1-\gamma}}{\mathscr{M}_{*}}(\dot{Q}_{N} - \dot{Q}_{V}), \tag{4.15}$$

while the temperature is given by

$$T = T_{*}\frac{\Psi}{\Psi_{*}}|\mathbf{q}|^{1-\gamma}. \tag{4.16}$$

From now on and throughout the paper we shall neglect the nuclear power $\dot{Q}_{N}$, an approximation which can be shown to be valid at least until the very high temperature phase that can be attained for sufficiently high values of the penetration factor (see CL83). The inclusion of such a contribution would involve the detailed treatment of thermonuclear reactions in the bulk of the star, a much more complicated problem that will be treated in a forthcoming paper (Luminet and Pichon 1986). Moreover, we shall neglect until § VI the dissipative work rate contribution, reducing our attention to strictly conservative variations.

The idealized polytropic affine star model will be appropriate in particular for the treatment of small main-sequence stars, for which we may use the nonrelativistic, nondegenerate monatomic gas formulae

$$\gamma = 5/3, \qquad \psi(\sigma) \propto \exp(2\sigma/3). \tag{4.17}$$

c) *The Standard Affine Star Model*

For medium and large main-sequence stars, the nonrelativistic polytropic treatment will be inadequate, but it will still be a good approximation over a wide range of temperatures to treat the stellar material as a mixture of a nonrelativistic, nondegenerate monatomic gas of particles with mass density ρ, together with a gas of blackbody radiation, so that the energy density will be expressible reasonably accurately by

$$\mathscr{E} = \frac{3}{2}\frac{k}{\mu m_{p}}\rho T + aT^{4}, \tag{4.18}$$

where k is the Boltzmann constant, a is the radiation constant, m_p is the proton mass, and μ is the mean molecular weight ($\mu = \frac{1}{2}$ for pure ionized hydrogen). The corresponding pressure is then given by

$$P = \frac{k}{\mu m_p} \rho T + \frac{1}{3} a T^4, \tag{4.19}$$

and the entropy per unit mass by (to an additive constant)

$$\sigma = \frac{k}{\mu m_p} \ln\left(\frac{T^{3/2}}{\rho}\right) + \frac{4a}{3} \frac{T^3}{\rho}. \tag{4.20}$$

It is convenient to introduce the auxiliary variable χ defined as

$$\chi = \frac{4a}{3} \frac{\mu m_p}{k} \frac{T^3}{\rho}, \tag{4.21}$$

which is to be interpreted as the photon entropy per nonrelativistic particle number ratio.

The polytropic values (4.7) and (4.8) are easily obtained from these latter expressions: at the limit $\chi \ll 1$ (low temperatures, high densities), one recovers the nonrelativistic ($\gamma = 5/3$) polytropic equation of state, while for $\chi \gg 1$ one obtains the purely relativistic ($\gamma = 4/3$) polytropic case.

The *adiabatic* equation of state is determined by the condition that the entropy per unit mass σ has a constant value, which may be expressed by

$$\sigma = \frac{k}{\mu m_p} \ln\left(\frac{3}{4a} \frac{\mu m_p}{k} \frac{1}{T_0^{3/2}}\right), \tag{4.22}$$

where the constant T_0 is interpretable as a critical temperature below which the entropy ratio χ is small compared with unity, since it can be seen from equations (4.21) and (4.22) that χ is given as a function of temperature by

$$\frac{T}{T_0} = \chi^{2/3} \exp\left(\frac{2}{3}\chi\right) \tag{4.23}$$

The quantity χ itself is given implicitly as a function of the density by

$$\frac{\rho}{\rho_0} = \chi \exp(2\chi), \tag{4.24}$$

where ρ_0 is analogously defined as a critical density below which χ becomes negligible, given by

$$\rho_0 = \frac{4a}{3k} T_0^3. \tag{4.25}$$

Substitution into equations (4.18) and (4.19) gives the corresponding expressions for the energy density and pressure in terms of the entropy ratio χ:

$$\mathscr{E} = a T_0^4 (2+\chi) \chi^{5/3} \exp\left(\tfrac{8}{3}\chi\right), \tag{4.26}$$

$$P = \tfrac{1}{3} a T_0^4 (4+\chi) \chi^{5/3} \exp\left(\tfrac{8}{3}\chi\right). \tag{4.27}$$

Unlike the simple polytropic formulae (4.7) and (4.8), these mixed formulae do not admit simple explicitly integrated expressions for the global internal energy and pressure integrals as functions of the deformation matrix q_{ia}, unless one is prepared to impose, as an additional simplifying assumption, the requirement that the equilibrium state value of χ, say χ_*, be *uniform* over the volume of the star model. Such a simplification is the basis of the so-called Eddington *standard* model (see, e.g., Cox and Giuli 1968, chap. 23), which played a fundamental role in the development of the theory of stellar structure as being a good approximation for chemically homogeneous stars that are not completely convective. From equation (4.24), the uniformity of χ_*

ensures the uniformity of χ in an adiabatically perturbed standard affine model, its value being given in terms of the corresponding deformation matrix by (using eq. [2.5])

$$\chi \exp(2\chi) = \chi_* \exp(2\chi_*)|\mathbf{q}|^{-1}. \tag{4.28}$$

Under these conditions substitution of equations (4.26) and (4.27) in the integral formulae (2.15) and (2.16) for the total internal energy and pressure integral leads to expressions of the form

$$\frac{U}{U_0} = (2+\chi)\chi^{2/3} \exp\left(\frac{2}{3}\chi\right), \tag{4.29}$$

$$\frac{\Pi}{\Pi_0} = (4+\chi)\chi^{2/3} \exp\left(\frac{2}{3}\chi\right), \tag{4.30}$$

where Π_0 and U_0 are functionals only of the entropy distribution σ; they are given by

$$\Pi_0 = \tfrac{1}{3} U_0 = \tfrac{1}{4} N_* k \bar{T}_0, \tag{4.31}$$

where N_* is the total number of nonrelativistic particles in the star and $\bar{T}_0 = \int T_0 \, dM$ is to be interpreted as the mass-averaged mean of the local value of T_0 over the star model.

We conclude this section by noting that, according to the Eddington formula for the (chemically homogeneous) standard model, the appropriate value of χ_* (which is related to the ratio β_g of nonrelativistic gas pressure to total pressure by $4/\beta_g = \chi_* + 4$) is given roughly in terms of the stellar mass by

$$\frac{M_*}{M_\odot} \approx \mu^{-2} \chi^{1/2}{}_*(\chi_* + 4)^{3/2}, \tag{4.32}$$

where $M_\odot$ is the solar mass value.

It can be seen that for typical chemical composition ($\mu \sim 0.6$ for a mixture of hydrogen and helium in solar abundances) and except for the very massive—and short-lived—stars with $M_* \gtrsim 30\ M_\odot$, the equilibrium value χ_* will be small compared with unity and is given approximately by

$$\chi_* \approx (M_*/30\ M_\odot)^2. \tag{4.33}$$

However, equation (4.28) shows that even for moderately massive stars, the variable χ may well increase above unity in the course of compression of the star within the Roche radius, when the volume factor $|\mathbf{q}|$ becomes small enough. One can therefore expect substantial departures from the polytropic estimates during the phase of maximum pancake compression.

In the range of very low stellar masses (say $M_* \leq 0.1\ M_\odot$), the photonic corrections are always totally negligible, but then it would be appropriate to introduce corrections due to the partial degeneracy of electrons (Pichon 1986).

V. NUMERICAL RESULTS FOR THE ADIABATIC AFFINE MODEL

a) *Nondisruptive/Disruptive Encounters*

With a view to numerical integration, the system of nine second-order differential equations (2.6) can be conveniently transformed into a system of 18 first-order equations of the form

$$\begin{aligned} \dot{Y}_i &= Y_{i+9} && \text{for } i = 1,\ldots,9, \\ \dot{Y}_i &= C_{ij} q_{ja} + \frac{\Pi_*}{\mathscr{M}_*}\left[\frac{\Pi}{\Pi_*} q_{ai}^{-1} - \frac{3}{2}\int_0^\infty du \frac{(\mathbf{S}+u\mathbf{1})_{ji}^{-1}}{|\mathbf{S}+u\mathbf{1}|^{1/2}} q_{ja}\right] && \text{for } i = 10,\ldots,18, \end{aligned} \tag{5.1}$$

with the correspondence

$$\begin{aligned} &Y_1 = q_{11}, \quad Y_2 = q_{12}, \quad Y_3 = q_{13}, \quad \ldots, \quad Y_9 = q_{33}, \\ &Y_{10} = \dot{q}_{11}, \quad Y_{11} = \dot{q}_{12}, \quad Y_{12} = \dot{q}_{13}, \quad \ldots, \quad Y_{18} = \dot{q}_{33}. \end{aligned}$$

If we neglect the minor corrections due to a conceivable initial spin of the star not orthogonal to the orbital plane, the number of degrees of freedom of the system reduces to five, since the angular velocity vector w and the shear vector ζ are then specified by their Z-component alone (using the terminology of the Riemann ellipsoids, the resulting affine configurations may be said to be of "type S"). It follows that there is complete decoupling between the motion orthogonal to the orbital plane (specified by component q_{33}) and the motion projected into the orbital plane, the components 13, 23, 31, 32 of the deformation matrix q_{ij} and of the velocity matrix $\dot{q}_{ij}$ being trivially zero. The system (5.1) reduces to a set of 10 independent first-order differential equations.

The numerical algorithm used for solving this system was a predictor-corrector "stiff" method and was performed on a VAX-11/780 computer.

The ratio $\Pi_*/\mathscr{M}_*$ may be used to fix the internal time scale of the star, so that

$$\tau_* = \left(\frac{\Pi_*}{\mathscr{M}_*}\right)^{-1/2}, \tag{5.2}$$

which is of the same order as the orbital time scale passed by the star within the Roche radius (a few hundred seconds for a solar-type star).

A characteristic Roche limit may thus be defined conventionally by

$$R_{\mathrm{R}} = \tau_*^{-2/3}(GM)^{1/3}. \tag{5.3}$$

Introducing the *penetration factor*

$$\beta = R_{\mathrm{R}}/R_p, \tag{5.4}$$

one sees that the maximal characteristic value of the tidal field (at the instant of passage at periastron) is merely given by

$$C_{\max} = \beta^3 \tau_*^{-2}. \tag{5.5}$$

Runs have been performed for β ranging from 0.16 up to 60. Figures 7*a*–7*f* show in the nonrelativistic ($\gamma = 5/3$) polytropic case the influence of the penetration factor on the evolution of the star configuration in the course of its orbital motion. The disruption is found to occur if the penetration factor is greater than the critical value $\beta_{\mathrm{cr}} = 0.465$, which corresponds to an *effective Roche limit* given by

$$R_{\mathrm{cr}} = 2.15\tau_*^{-2/3}(GM)^{1/3}. \tag{5.6}$$

If we define the mean characteristic density of the spherical configurations as that of the homogeneous model with the same mass M_* and radius R_* (i.e., given by eq. [3.3]), we obtain

$$R_{\mathrm{cr}} = 1.924\left(\frac{M}{\rho_*}\right)^{1/3}. \tag{5.7}$$

By comparing with the disruption limit (3.6) for the incompressible fluid model, one recovers the expected property that the compressibility tends to decrease the stability of a self-gravitating body, i.e., tends to increase (albeit slightly) the effective Roche limit above its incompressible value (the effect of "static tidal decompression" is ultimately responsible for the overflow phenomenon in tight binary systems).

When $\beta < \beta_{\mathrm{cr}}$, as in the incompressible case, the maximum tidal perturbation (5.6) is not sufficient to destroy the star model, but oscillations of the principal axes, angular momentum, and vorticity develop (Figs. 7*a*, 7*b* and 8*a*, 8*b*). The initial spherical configuration bifurcates toward a sequence of (irrotational) *stationary configurations* that are *conformal* to the incompressible Riemann ellipsoids of type S (i.e., they are directly obtainable from the latter by a mere scale factor; see CL85) (Fig. 9).

For *weakly disruptive encounters*, i.e., when $\beta_{\mathrm{cr}} \leq \beta \lesssim 1$, the affine star model evolves to a more and more elongated *cigar-like* configuration (Fig. 7*c*). In this range of periastron distances the behavior of the affine star model is roughly similar to that of the incompressible model (except for the inevitable effect of volume augmentation), since the star does not penetrate enough into the effective Roche limit to undergo an important squeezing.

In contrast, as soon as the penetration factor increases significantly above unity, say $\beta \gtrsim 5$ (*strongly disruptive encounters*), the tidal effects are strongly compressive in the Z-direction when the star penetrates within the Roche radius, so that a transitory, highly flattened *pancake* configuration develops just after the passage at the periastron, in accordance with our previous predictions (CL82). Of course the flattening is finally halted by the sudden buildup of pressure forces, and the further fate of the affine star model remains expansion and disruption (Figs. 7*d*, 7*e*, 7*f* and 10*a*, 10*b*).

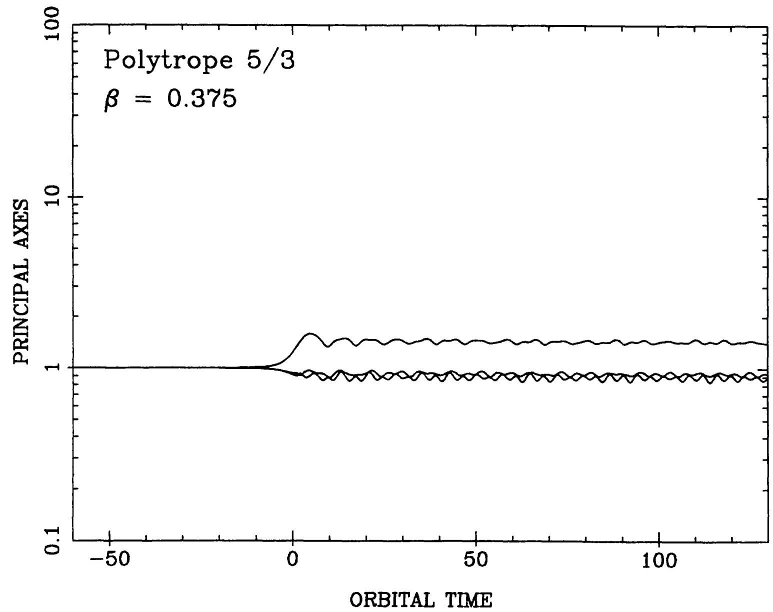

FIG. 7*a*

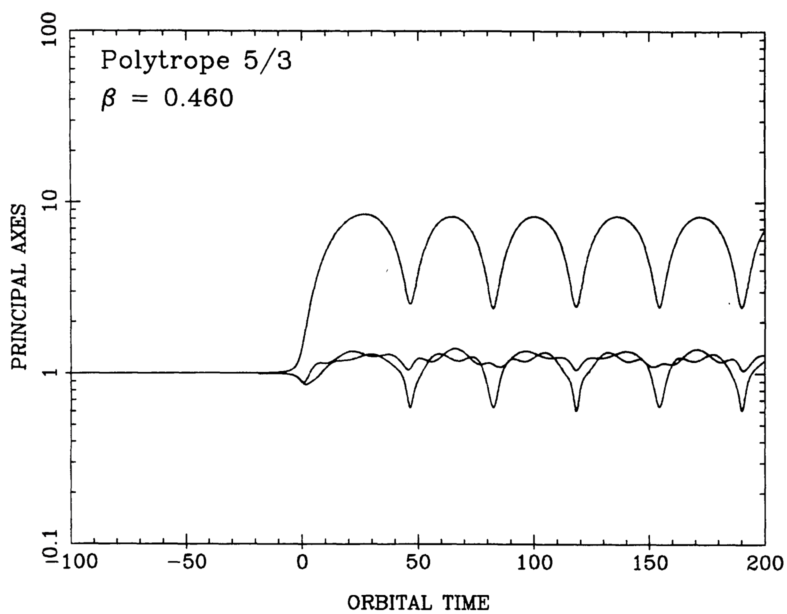

FIG. 7*b*

FIG. 7.—Ellipsoidal deformations of the adiabatic affine star model. The equation of state is polytropic with index 5/3; the penetration factor β varies from 0.375 to 50. As in Figs. 1–6 illustrating the incompressible case, the orbital time scale is in units of the internal timescale τ_*. The variation of the principal axes is shown in logarithmic scale (axis a_3 corresponding to the direction orthogonal to the orbital plane). ($a-b$) Nondisruptive encounters. The star is not broken, but its configuration evolves from the undistorted sphere toward a Riemann stationary solution. (c) Weakly disruptive encounter. The compression effects are very mild; the configuration evolves quickly toward an indefinitely elongated cigar with $a_1 \gg a_2 \approx a_3$. ($d-f$) Strongly disruptive encounters. The transitory formation of a pancake configuration appears soon after periastron; the final configuration is more isotropic, with $a_1 \gtrsim a_3 > a_2$. The dashed vertical lines represent the instants of passage (in and out) at the Roche radius.

In such a high temperature and density phase, the equation of state of the stellar gas may come into play. We have thus also integrated the equations of deformation for the relativistic ($\gamma = 4/3$) polytropic and for the standard affine star model. Figure 11 shows the time evolution of the entropy ratio $\chi(t)$ in the case of a standard affine model with mass $M_* = 3\ M_\odot$ and penetration factor $\beta = 15$. If throughout the motion of the star model the entropy ratio $\chi(t)$ remains smaller than unity, the effects of radiation may be neglected and the polytropic model with $\gamma = 5/3$ is a very good approximation. Figure 12 depicts the regions in the (β, M_*)-plane where the standard model must be used instead of the simpler polytropic one.

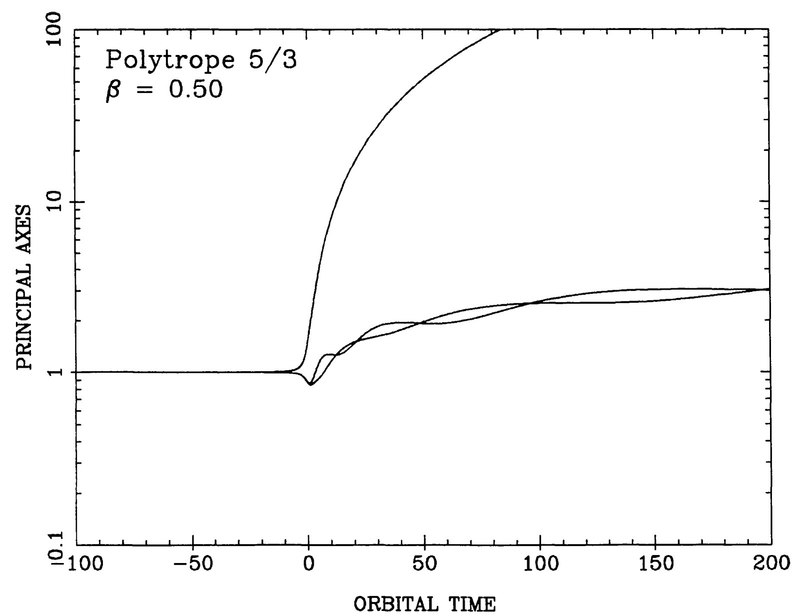

FIG. 7*c*

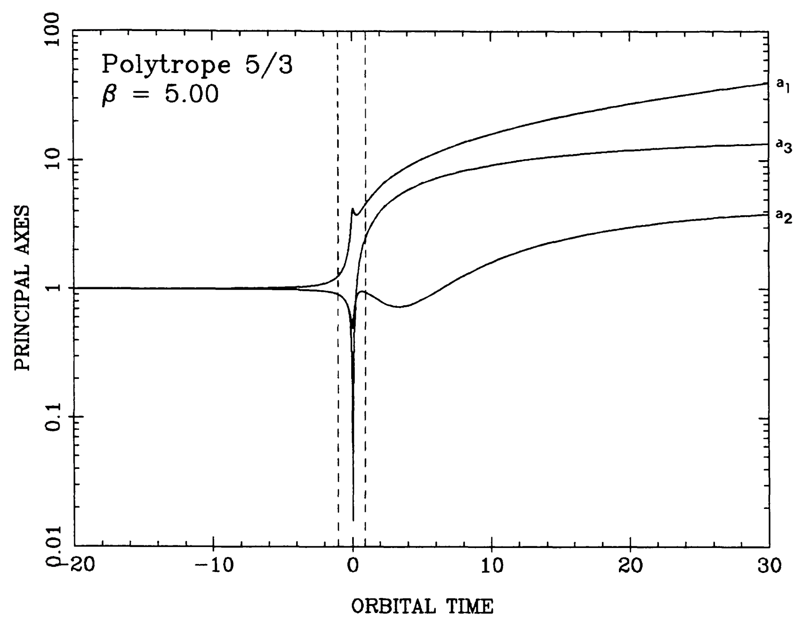

FIG. 7*d*

b) Characteristic Pancake Quantities

With a view to subsequent consideration of the nuclear reactions that can be triggered in the bulk of the star, particular interest attaches to the extremal values of the density and of the temperature attained in the pancake configuration. Let us recall that previous analytical investigation (CL83) led to the conclusion that, since the maximum "pancake" thermal energy U_m comes from the conversion of the kinetic energy of vertical motion, i.e.,

$$U_m \approx \tfrac{1}{2}\mathcal{M}_* \dot{q}_{33}^2 , \tag{5.8}$$

and given the fact that the maximum compression velocity $|\dot{q}_{33}|$ at the end of the free-fall motion is of the order of β, the maximum internal energy is merely given approximately by

$$U_m \approx \beta^2 U_* . \tag{5.9}$$

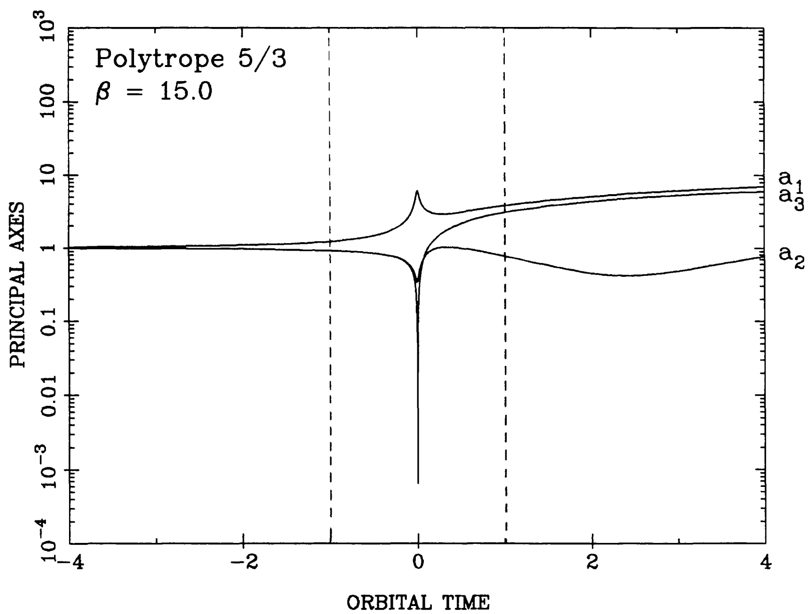

FIG. 7*e*

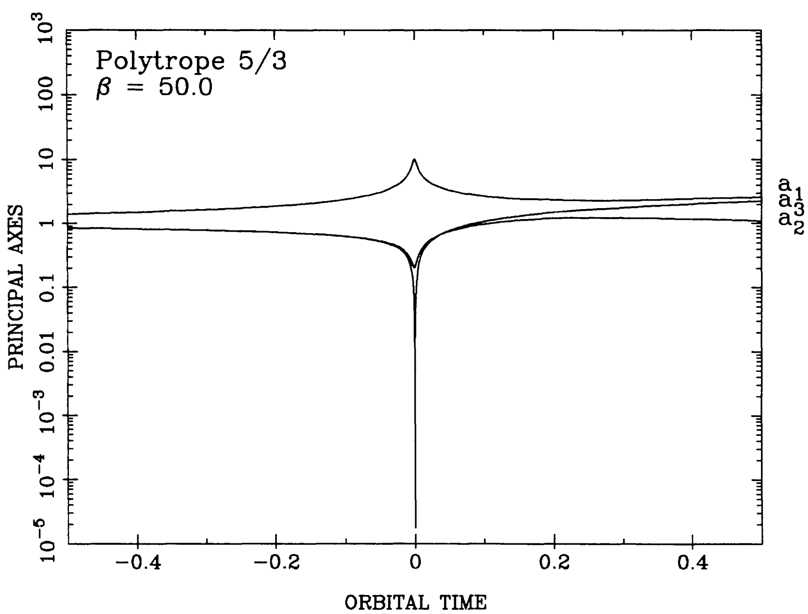

FIG. 7*f*

For the polytropic equation of state we deduced immediately the order-of-magnitude estimates

$$\frac{T_m}{T_*} \approx \beta^2, \qquad \frac{\rho_m}{\rho_*} \approx \beta^{2/(\gamma-1)}. \tag{5.10}$$

The present numerical calculations allow a more accurate specification of efficiency factors for strongly disruptive encounters (when shocks are neglected):

$$\frac{T_m}{T_*} = 0.37\beta^2, \qquad \frac{\rho_m}{\rho_*} = 0.22\beta^3 \qquad \text{for } \gamma = 5/3, \tag{5.11a}$$

$$\frac{T_m}{T_*} = 0.19\beta^2, \qquad \frac{\rho_m}{\rho_*} = 0.007\beta^6 \qquad \text{for } \gamma = 4/3. \tag{5.11b}$$

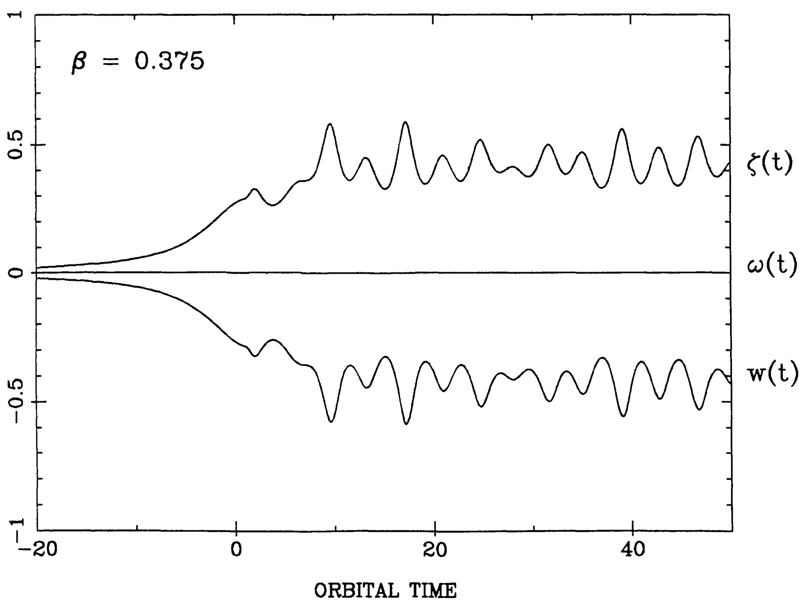

FIG. 8a

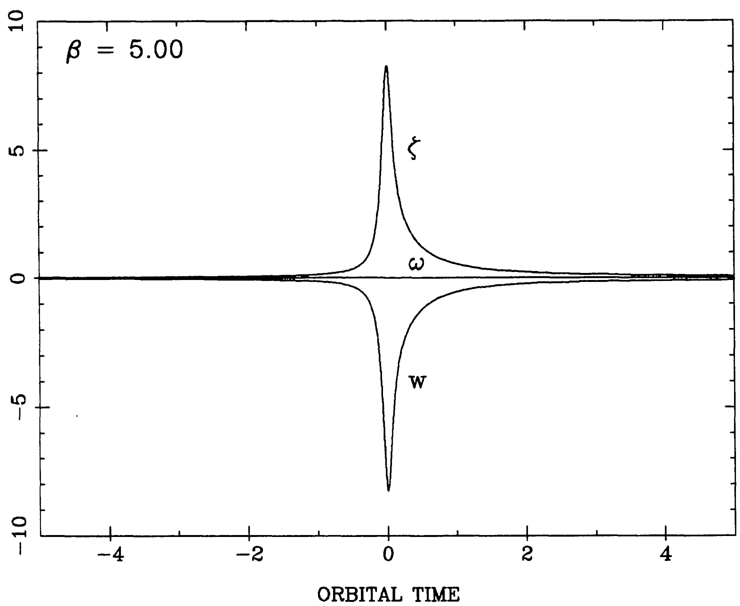

FIG. 8b

FIG. 8.—Internal motions induced by tidal effects in the affine star model. As in Fig. 1b for the incompressible case, we have depicted the time variations of the angular velocity vector $\boldsymbol{w}$, the shear vector $\boldsymbol{\zeta}$ and the rotation vector $\boldsymbol{\omega} \equiv \boldsymbol{w} + \boldsymbol{\zeta}$. (a) $\beta = 0.375$ (nondisruptive); (b) $\beta = 5.000$ (disruptive).

The characteristic duration of the pancake phase (defined as the time scale during which the temperature remains close to its maximum value by a factor of, say, 2) is given by

$$\Delta t_m \approx 10\beta^{-4}\tau_* \qquad \text{for } \gamma = 5/3, \tag{5.12a}$$

$$\Delta t_m \approx 420\beta^{-7}\tau_* \qquad \text{for } \gamma = 4/3. \tag{5.12b}$$

The nonrelativistic ($\gamma = 5/3$) polytropic formulae will remain valid as long as the mass of the star model is sufficiently low for the

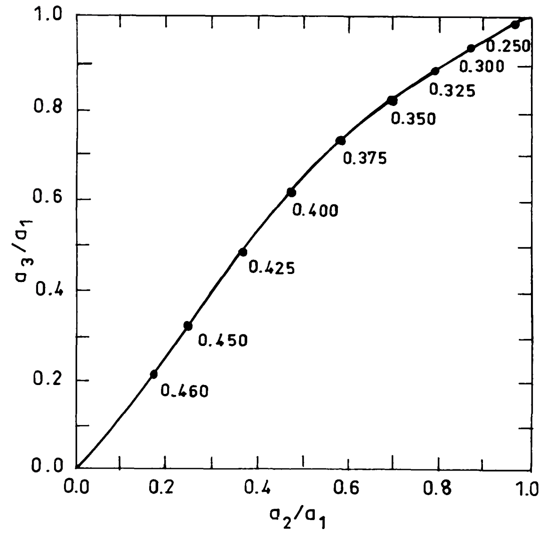

FIG. 9.—Irrotational polytropic Riemann sequence. Nondisruptive encounters ($\beta < 0.465$) transform a sphere into an ellipsoidal configuration oscillating around a stationary solution belonging to a conformal Riemann sequence (here the polytropic sequence with $\gamma = 5/3$), which is irrotational (owing to conservation of the vorticity in the absence of dissipation), and characterized by axis ratios $a_2/a_1, a_3/a_1$ identical with those of the irrotational incompressible Riemann sequence. Points in the picture are labeled by the corresponding values of the penetration factor.

entropy ratio χ to reach a maximum value χ_m smaller than unity:

$$\chi_m \approx \chi_* \left(\frac{T_m}{T_*} \right)^{3/2} \lesssim 1 . \tag{5.13}$$

Using the approximate relation (4.32) between χ_* and the stellar mass M_*, we obtain the upper mass limit condition

$$M_* \lesssim 25 \ M_\odot \left(\frac{T_m}{T_*} \right)^{-3/4} , \tag{5.14}$$

which turns out to be $\sim 0.8 \ M_\odot$ for the characteristic heating factor of 100 (at which efficient explosive helium burning is likely to occur; see CL82 and Pichon 1985).

When this condition is violated, we should still be able to recover reasonably satisfactory results by using the standard model, according to which χ_m is given implicitly (from eqs. [4.29] and [5.9] by

$$\frac{2+\chi_m}{2+\chi_*} \left(\frac{\chi_m}{\chi_*} \right)^{2/3} \exp \frac{2}{3} (\chi_m - \chi_*) \approx \beta^2 . \tag{5.15}$$

In this case the maximum pancake temperature and density will be given by

$$\frac{T_m}{T_*} \approx \frac{2+\chi_*}{2+\chi_m} \beta^2 , \qquad \frac{\rho_m}{\rho_*} = \frac{\chi_*}{\chi_m} \left(\frac{T_m}{T_*} \right)^3 . \tag{5.16}$$

Since (from eqs. [4.23] and [4.24]) $d(\ln T)/d(\ln \rho) = \frac{2}{3}(1+\chi)/(1+2\chi)$, for a given density the temperature of the standard model is intermediate between the $\gamma = 5/3$ and $\gamma = 4/3$ polytropic values. But since for a given (sufficiently high) penetration factor β the compression factor will itself be intermediate between its $\gamma = 5/3$ and $\gamma = 4/3$ polytropic values, it is clear that the law of maximum heating $T_m(\beta)$ may even drop below the photonic ($\gamma = 4/3$) case at some stage of the compression. This can also be seen directly from equation (5.16) at the limit $\beta \gg 1$, and is clearly illustrated by the numerical results of Figure 13.

At this stage the reader may rightfully question the validity of the affine approximation for the determination of extremal pancake quantities. First it is clear that the affine model cannot account for the fine spatial structure of the star just at the instant of maximum compression: as was emphasized by Bicknell and Gingold (1983), the real configuration looks rather like a tube of toothpaste squeezed at the point of maximum compression (fixed on the orbit); anyway, because the orbital velocity of the star near periastron (comparable to the velocity of light in the vicinity of the black hole horizon) is much greater than the sound velocity, the effect of nonsimultaneity of the squeezing cannot very much affect the affine estimates of ρ_m and T_m. However, the

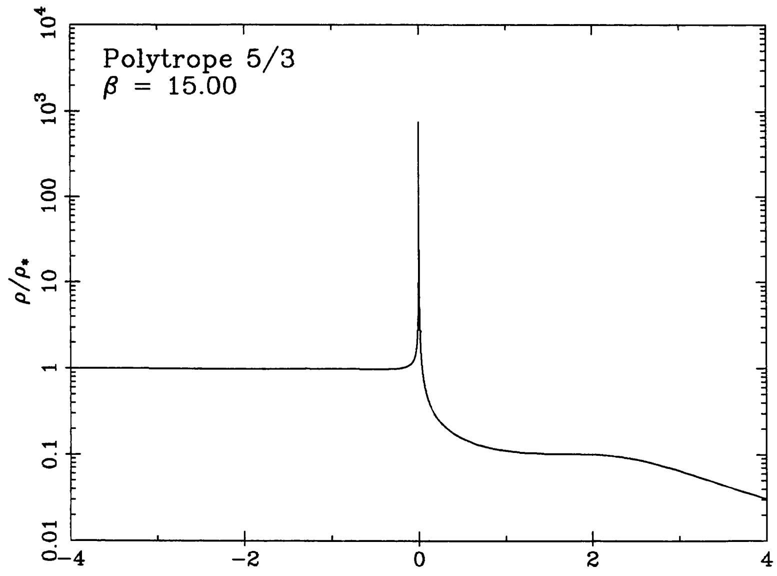

FIG. 10a

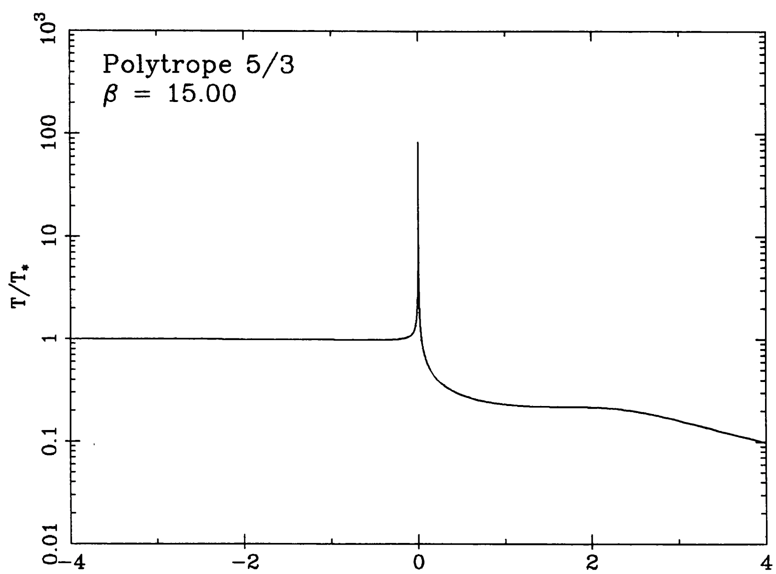

FIG. 10b

FIG. 10.—Time variations of (a) density ρ/ρ_* and (b) temperature T/T_* (in logarithmic scale), for a penetration factor $\beta = 15$ and the polytropic equation of state $\gamma = 5/3$.

inadequacy of the affine approximation for describing the outer layers of the star imposes much more severe restrictions on the credibility of the model. In effect, the outer layers of a more realistic star, being less dense than the central bulk, will be liberated sooner in the external tidal field; it is therefore plausible that shock waves develop in the course of the compression to a sufficient extent to reverse the collapse of the envelope. If this occurs soon enough, it could easily reduce the maximum density.

Starting with this idea, Bicknell and Gingold (1983) have treated in the "smoothed particle hydrodynamics" approximation the problem of tidal encounters between polytropic stars and large black holes. They concluded that the affine values for the maximum compression were overestimated by up to several orders of magnitude. However, it is well known that in such hydrodynamical simulations the numerical treatment requires the introduction of an *artificial viscosity*. This is why the last section of this paper will deal with the effects of viscosity terms on the behavior of the affine star model.

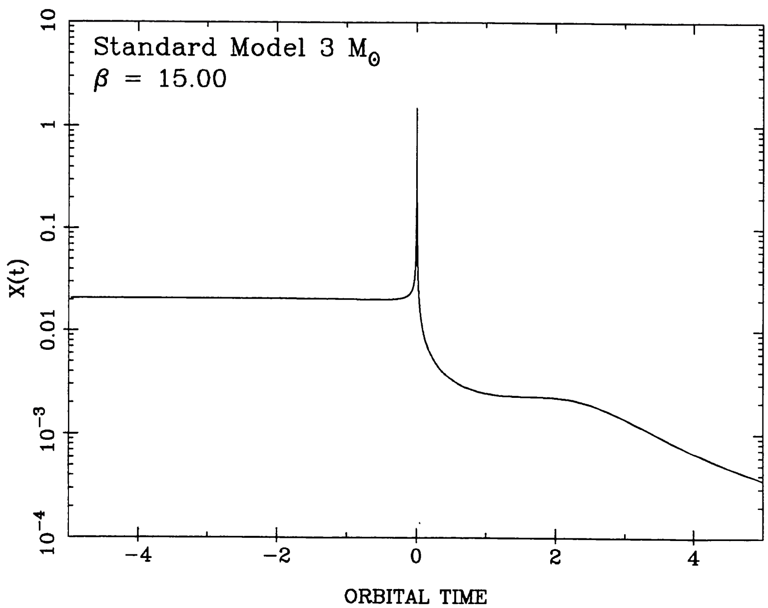

FIG. 11.—Time variation of the entropy ratio χ for a penetration factor $\beta = 15$ and a standard equation of state with stellar mass $M_* = 3\ M_\odot$ (which fixes the equilibrium value of the photon entropy ratio χ_* to 2.0×10^{-2}). During the compression phase, the entropy ratio χ increases above unity, so that the star becomes dominated by radiation in its pancake configuration.

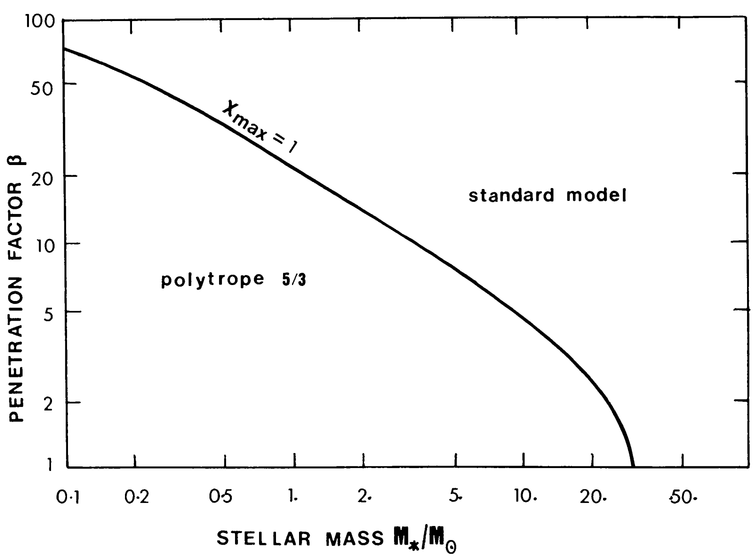

FIG. 12.—Domain of application of the standard model in terms of the stellar mass and the penetration factor. In the region above the curve $\chi_m = 1$, the star is dominated by radiation and the standard model has to be used. For ordinary stellar masses ($M_* \lesssim 1\ M_\odot$), the nonrelativistic polytropic model is a very good approximation.

FIG. 13.—Influence of the equation of state on the extremal pancake quantities: (a) density (compression factor); (b) temperature (heating factor). The different curves correspond respectively to the polytropic models $\gamma = 5/3$ and $\gamma = 4/3$ (*dashed line*) and the standard models with mass $M_* = 3\ M_\odot$, 15 $M_\odot$. When $\beta \gtrsim 5$, the pancake density and the pancake temperature vary roughly as β^p, where p depends on the equation of state. For a given penetration factor, the compression factor of the standard models lie between the compression factors of the polytropic models 4/3 and 5/3, while the heating factor may even drop below the purely relativistic case $\gamma = 4/3$.

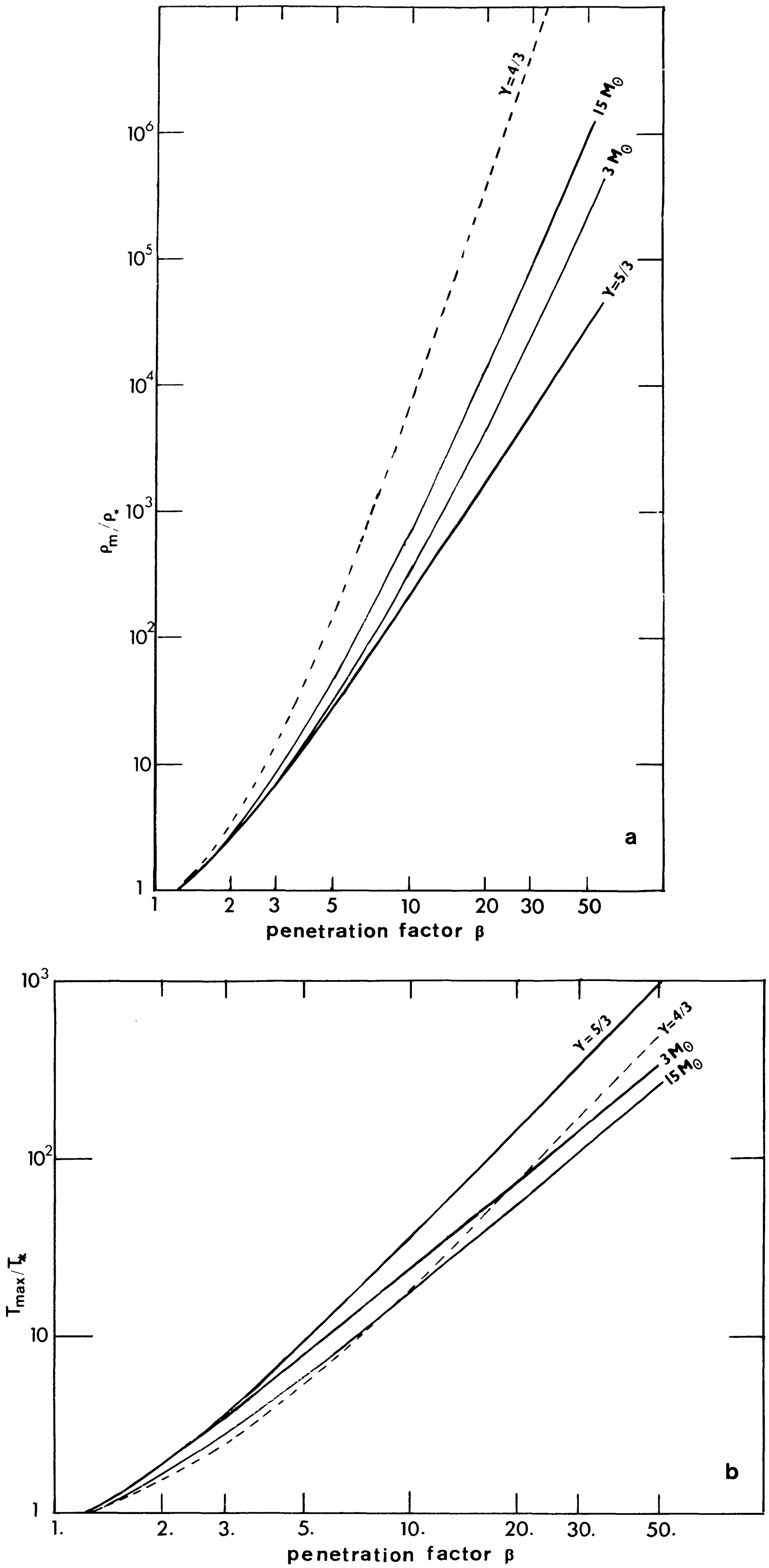
γ=4/3
15 M⊙
3 M⊙
γ=5/3
ρ_m/ρ_*
a
penetration factor β
γ=5/3
γ=4/3
3 M⊙
15 M⊙
T_{max}/T_*
b
penetration factor β

FIG. 13

VI. THE VISCOUS POLYTROPIC AFFINE MODEL

In this section we turn again to the simple nonrelativistic polytropic affine model, but we introduce a supplementary *dissipative* force contribution as originated from a stress viscosity tensor z_{ij} of the standard form

$$z_{ij} = 2\rho\nu\left(\theta_{ij} - \tfrac{1}{3}\theta\delta_{ij}\right) + \rho\lambda\theta\delta_{ij}, \tag{6.1}$$

where

$$\theta_{ij} = \tfrac{1}{2}\left(\dot{q}_{ia}q_{aj}^{-1} + \dot{q}_{ja}q_{ai}^{-1}\right) \tag{6.2}$$

is the symmetric divergence tensor whose trace θ is the ordinary flow divergence, ν is the kinematic shear viscosity coefficient, and λ is the kinematic bulk viscosity coefficient. From equation (2.21), the dissipative internal force moment Σ_{ij} appearing in the general equations of motion (2.6) can be expressed as

$$\Sigma_{ij} = 2\mathscr{Y}\theta_{ij} + \left(\mathscr{X} - \tfrac{2}{3}\mathscr{Y}\right)\theta\delta_{ij}, \tag{6.3}$$

where

$$\mathscr{Y} = \int \nu \, dM, \qquad \mathscr{X} = \int \lambda \, dM \tag{6.4}$$

are the corresponding global viscosity coefficients.

The nonadiabatic part of the gas energy variations (in the absence of nuclear sources) is expressible as

$$\frac{\partial U}{\partial t} = -\Sigma_{ij}\theta_{ij}. \tag{6.5}$$

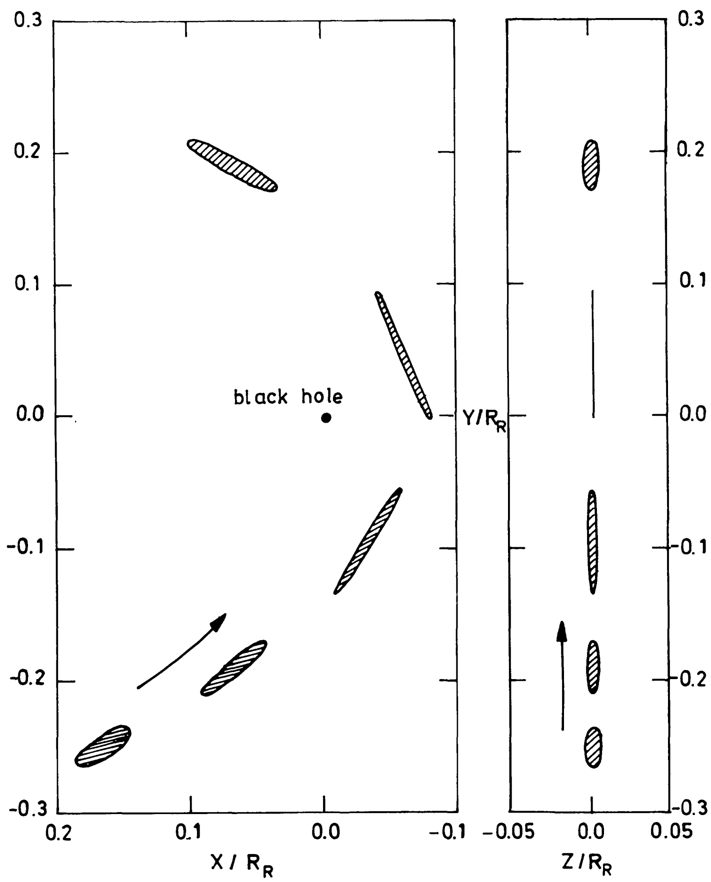

FIG. 14.—Deformations of the viscous affine star model penetrating deeply within the tidal field of a black hole. The picture arises from numerical integration of the equations of motion along a parabolic orbit with penetration factor $\beta = 16$. For the sake of clarity, the size of the star relative to the orbital distance scale (in units of the Roche distance) has been considerably emphasized. *Left*: Ellipsoidal configurations as projected in the orbital (X, Y)-plane. The area of the section remains practically constant between the instants of passage within the Roche radius and at periastron, owing to the rotation of the principal directions of the tidal tensor. *Right*: Ellipsoidal configurations in the direction orthogonal to the orbital plane. The result is identical with that of Fig. 1 of Bicknell and Gingold (1983), which is based on a smooth particle hydrodynamics approximation.

From equation (4.15) it follows that the entropy distribution integral satisfies the differential equation

$$\dot{\Psi} = \frac{|\mathbf{q}|}{\mathscr{M}_*}^{2/3} \Sigma_{ij}\theta_{ij}, \tag{6.6}$$

while the temperature is given by

$$\frac{T}{T_*} = \frac{\Psi}{\Psi_*}|\mathbf{q}|^{-2/3}. \tag{6.7}$$

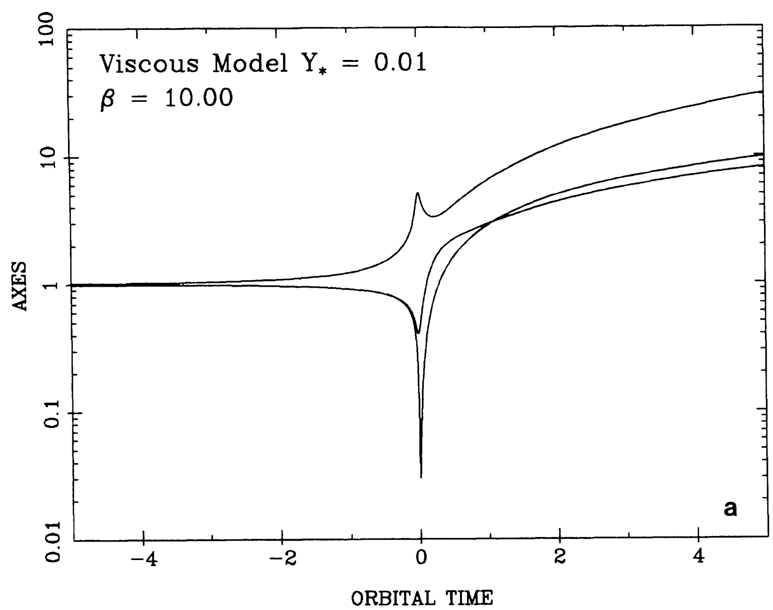

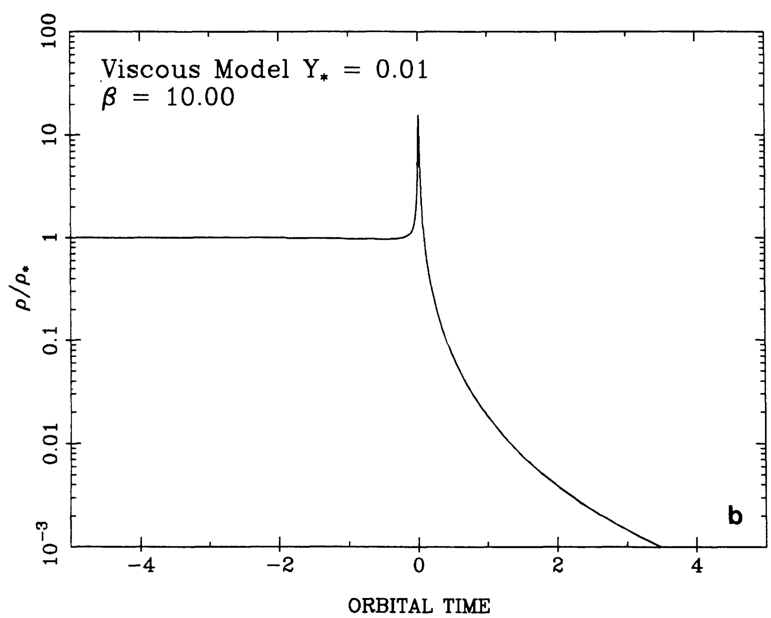

FIG. 15.—Mechanical evolution of the viscous affine model. The equation of state is polytropic ($\gamma = 5/3$), the penetration factor is $\beta = 10$, and the coefficient of shear viscosity is $\mathscr{Y}_* = 0.01$ (see text for units). (a) Principal axes a_i; (b) density ρ/ρ_*; (c) vertical compression velocity v/v_*; (d) entropy integral Ψ/Ψ_*; (e) temperature T/T_*.

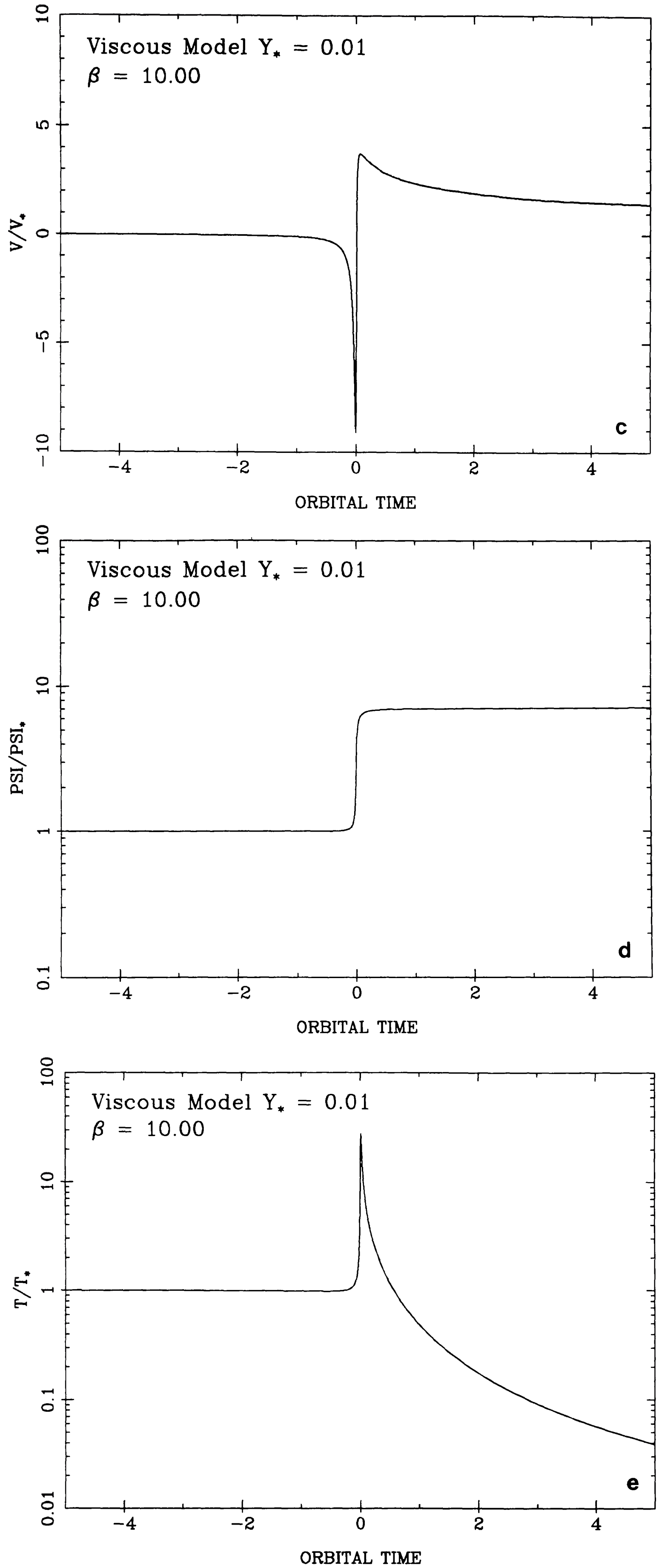

FIG. 15.—*Continued*

(This last equation shows clearly that the compressional energy depending on $|\mathbf{q}|^{-2/3}$ and the viscosity heat can both contribute to the total heating of the gas.)

One has still to specify the expression of viscosity coefficients as functions of local conditions such as entropy and density. A particularly simple model (exemplified by the case of a perfect monatomic gas) can be specified by taking the shear viscosity ν as proportional to $T^{1/2}\rho^{-1}$ while the bulk viscosity is zero, so that we obtain the integral relations

$$\mathscr{Y} = \mathscr{Y}_*\left(\frac{\Psi}{\Psi_*}\right)^{1/2} |\mathbf{q}|^{2/3}, \qquad \mathscr{X} = 0. \tag{6.8}$$

The viscous polytropic affine model is now completely described by the set of 10 coupled equations of motion (2.6) and (6.6), together with laws (6.3) and (6.8) giving the dependence of the viscous force contribution in terms of $|\mathbf{q}|$ and Ψ.

As already alluded to above, the introduction of viscosity in the affine star model was done in order to simulate the artificial dissipative effects appearing generally in numerical treatment of hydrodynamic models. In such calculations, dissipation is introduced partly for the purpose of obtaining numerical stability and partly to allow the treatment of shocks. In the particular case of the smooth particle simulation of tidal disruption of a hydrodynamic star model by Bicknell and Gingold (1983), the artificial Lax-Wendroff type of dissipation mechanism was so effective in damping out spatial inhomogeneities that we were able to simulate their results with considerable accuracy (Fig. 14) using a simple affine model with dissipation specified by formulae of the form (6.3), (6.8) for appropriately chosen values of the constant $\mathscr{Y}_*$. Figures 15*a*–15*e* show, respectively, time variations of the principal axes, of the compression velocity, of the density, of the entropy, and of the temperature for a penetration factor $\beta = 10$ and the value $\mathscr{Y}_* = 0.01$ of the viscosity coefficient in units such that $GM = 1$, $\Pi_*/\mathscr{M}_* = 1$, $\Psi_*\mathscr{M}_* = 1$.

By comparison with the adiabatic case, it is clear that the vertical velocity is strongly damped and that the maximum density in the pancake phase is reduced by more than one order of magnitude. Figure 16 illustrates the nonconservation of the fluid circulation in the presence of shear viscosity (see CL85). Figures 17*a* and 17*b* show the dependence on the penetration factor of the maximum temperature and the maximum density for different values of $\mathscr{Y}_*$. As claimed by Bicknell and Gingold (1983), for very large values of the penetration factor the maximum density attained does not increase with increasing β, while the maximum temperature law is hardly modified from the purely adiabatic case.

In conclusion, the inclusion of adequately chosen viscosity within the affine framework allows us to simulate very faithfully the results of the smoothed particle calculation of Bicknell and Gingold. However, this striking example cannot be construed as evidence of high physical accuracy of the affine treatment: the agreement results merely from the fact that the more sophisticated hydrodynamical treatment may have been prevented by lack of resolution from achieving the higher accuracy of which it might potentially have been capable.

We are grateful to S. Bonazzola for interesting discussions and to B. Pichon for helpful assistance.

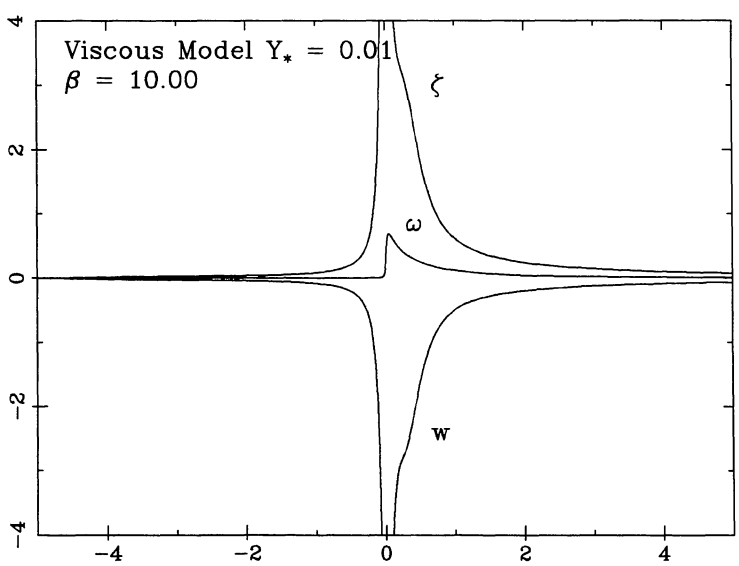

FIG. 16.—Internal motions in viscous affine model, illustrating the nonconservation of the vorticity in the presence of shear viscosity

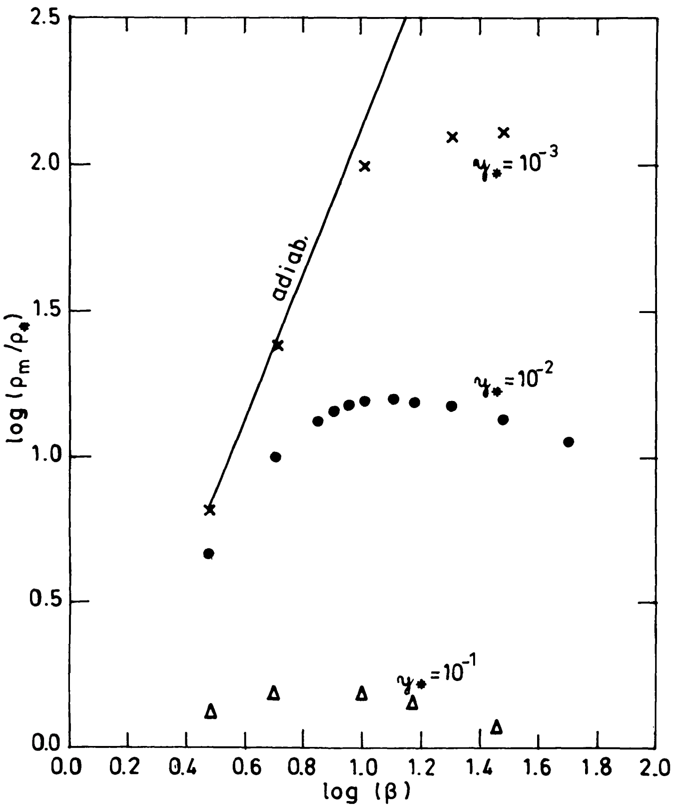

FIG. 17a

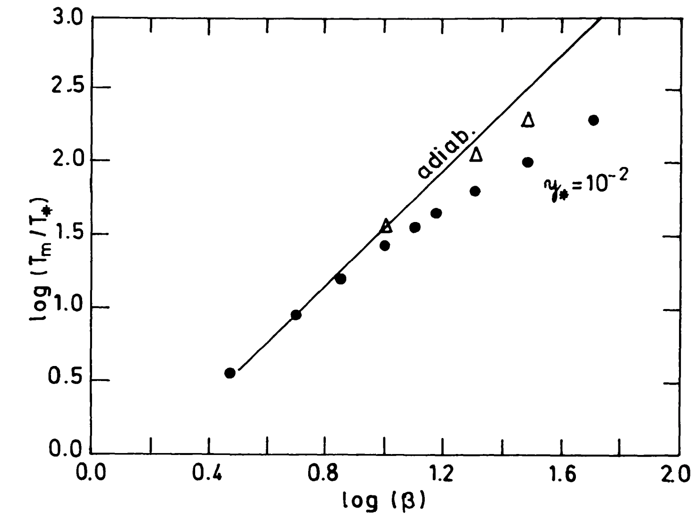

FIG. 17b

FIG. 17.—Influence of viscosity on (a) the maximum compression law and (b) the heating laws. The full line represents the nonviscous affine model. The temperature law is not very much modified. On the contrary, the compression law is no longer of the form β^p but decreases for high values of β, exactly as in the hydrodynamical simulation of Bicknell and Gingold (1983).

APPENDIX A

ALGEBRAIC COMPUTATION OF THE SELF-GRAVITATIONAL TENSOR COMPONENTS

When as in the present work there is complete decoupling between the "vertical" motion as represented by component q_{33} of the deformation matrix and the "equatorial" motion as represented by components $q_{11}, q_{12}, q_{21}, q_{22}$, the principal axes of the configuration are expressed as

$$a_1^2 = \tfrac{1}{2}\left(q_{11}^2 + q_{12}^2 + q_{21}^2 + q_{22}^2 + \delta^{1/2}\right), \tag{A1a}$$

$$a_2^2 = \tfrac{1}{2}\left(q_{11}^2 + q_{12}^2 + q_{21}^2 + q_{22}^2 - \delta^{1/2}\right), \tag{A1b}$$

$$a_3^2 = q_{33}^2, \tag{A1c}$$

$$\delta = \left[(q_{11} + q_{22})^2 + (q_{12} - q_{21})^2\right]\left[(q_{11} - q_{22})^2 + (q_{12} + q_{21})^2\right]. \tag{A1d}$$

In the star's center-of-mass frame, the self-gravitational energy tensor Ω_{ij} takes the form (2.18) involving the elliptic integrals A_{ij} defined by equation (2.19). The latter are functions only of the configuration matrix S defined by equation (2.4). It is clear that S_{ij} takes the diagonal form $S_{ij} = \sum_i a_i \delta_{ij}$ in the principal axis frame, so that the A_{ij} take the diagonal form $A_{ij} = \sum_i A_i \delta_{ij}$, where

$$A_i = a_1 a_2 a_3 \int_0^{\infty} \frac{du}{\left(a_i^2 + u\right)\Delta}, \tag{A2}$$

$$\Delta^2 = \left(a_1^2 + u\right)\left(a_2^2 + u\right)\left(a_3^2 + u\right). \tag{A3}$$

In the reference spherical configuration, the A_i are merely equal to $2/3$, and more generally in any triaxial configuration they satisfy the algebraic identity

$$A_1 + A_2 + A_3 = 2. \tag{A4}$$

By straightforward algebraic manipulations, the nonvanishing components of the tensor A_{ij} in the center-of-mass frame may be expressed as

$$A_{11} = A_1 + (\delta^{1/2} - q_{11}^2 - q_{12}^2) I_{12}, \tag{A5a}$$

$$A_{12} = A_{21} = -(q_{11}q_{21} + q_{12}q_{22}) I_{12}, \tag{A5b}$$

$$A_{22} = A_1 + (\delta^{1/2} - q_{22}^2 - q_{21}^2) I_{12}, \tag{A5c}$$

$$A_{33} = A_3, \tag{A5d}$$

with the A_i given by equation (A2) and

$$I_{12} = a_1 a_2 a_3 \int_0^\infty \frac{du}{(a_1^2 + u)(a_2^2 + u)\Delta}. \tag{A6}$$

For numerical calculations using standard subroutines, the elliptic integrals above are conveniently reduced to standard elliptic integrals of the first and second kind. From classical tables (Gradshteyn and Ryzhik 1980), we obtain effectively

$$A_1 = \frac{2a_1a_2a_3}{(a_1^2 - a_2^2)(a_1^2 - a_3^2)^{1/2}}[F(\nu, k) - E(\nu, k)], \tag{A7a}$$

$$A_3 = \frac{2a_1a_2a_3}{(a_3^2 - a_2^2)(a_1^2 - a_3^2)^{1/2}}E(\nu, k) + 2\frac{a_2^2}{a_2^2 - a_3^2}, \tag{A7b}$$

$$I_{12} = \frac{2a_1a_2a_3}{(a_2^2 - a_3^2)(a_1^2 - a_2^2)(a_1^2 - a_3^2)^{1/2}}[(a_1^2 + a_2^2 - 2a_3^2)E(\nu, k) + 2(a_3^2 - a_2^2)F(\nu, k)] - \frac{2a_3^2}{(a_2^2 - a_3^2)(a_1^2 - a_2^2)}, \tag{A7c}$$

where F and E are the elliptic integrals of the first and second kind with modulus k and argument ν, defined by

$$F(\nu, k) = \int_0^\nu (1 - k^2 \sin^2 \alpha)^{-1/2} d\alpha, \tag{A8a}$$

$$E(\nu, k) = \int_0^\nu (1 - k^2 \sin^2 \alpha)^{1/2} d\alpha, \tag{A8b}$$

$$k = [(a_1^2 - a_2^2)/(a_1^2 - a_3^2)]^{1/2}, \qquad \nu = \arcsin(1 - a_3^2/a_1^2)^{1/2}. \tag{A8c}$$

APPENDIX B

SPECIFICATIONS OF THE FLUID MOTIONS

In terms of the deformation matrix q_{ia} (corresponding to the center-of-mass frame coordinates r_i), the *spin* (intrinsic angular momentum) vector $\boldsymbol{J}$ and the (adjoint) vorticity vector $\boldsymbol{J}^\dagger$ are defined by (see CL85)

$$\frac{J_i}{\mathcal{M}_*} = \frac{1}{4}\varepsilon_{ijk}(q_{ja}\dot{q}_{ka} - \dot{q}_{ja}q_{ka}), \tag{B1a}$$

$$\frac{J_i^\dagger}{\mathcal{M}_*} = \frac{1}{4}\varepsilon_{ijk}(q_{aj}\dot{q}_{ak} - \dot{q}_{aj}q_{ak}), \tag{B1b}$$

where ε_{ijk} is the three-dimensional alternating tensor. Using the decoupling property already mentioned, $\boldsymbol{J}$ and $\boldsymbol{J}^\dagger$ can be specified by their 3-component alone (i.e., they remain orthogonal to the orbital plane).

The motion of the fluid relative to the center-of-mass frame is characterized by the *rotation* vector $\boldsymbol{\omega} \equiv \frac{1}{2}(\nabla \times \boldsymbol{v})$, whose nonzero component is given by

$$\omega_3 = \frac{1}{a_1 a_2} \frac{J_3^\dagger}{\mathscr{M}_*}. \tag{B2}$$

The angular velocity of the principal axis frame relative to the center-of-mass frame (denoted $\boldsymbol{\Omega}$ in the classical book by Chandrasekhar 1969) is thus

$$w_3 = \left[\tfrac{1}{2}\left(a_1^2 + a_2^2\right) J_3/\mathscr{M}_* + a_1 a_2 J_3^\dagger/\mathscr{M}_*\right] / \left[a_1^2 a_2^2 - \tfrac{1}{4}\left(a_1^2 + a_2^2\right)^2\right], \tag{B3}$$

while the angular velocity of the principal frame relative to the (spherical) reference frame with coordinates $\hat{r}_a$ (denoted Λ in Chandrasekhar 1969) is the adjoint quantity

$$w_3^\dagger = \left[\tfrac{1}{2}\left(a_1^2 + a_2^2\right) J_3^\dagger/\mathscr{M}_* + a_1 a_2 J_3/\mathscr{M}_*\right] / \left[a_1^2 a_2^2 - \tfrac{1}{4}\left(a_1^2 + a_2^2\right)^2\right]. \tag{B4}$$

Finally, the angular velocity of the fluid itself relative to the principal axis frame, referred to in the present paper as the shear vector, is

$$\zeta_3 = -\frac{1}{2} \frac{a_1^2 + a_2^2}{a_1 a_2} w_3^\dagger \tag{B5}$$

(the quantity denoted $\boldsymbol{\zeta}$ in Chandrasekhar 1969 and referred to as the "vorticity vector" is twice the present shear vector).

By adding the angular velocity of the fluid relative to the principal axis frame and the angular velocity of the principal frame relative to the center-of-mass frame, one recovers obviously the rotation rate vector, i.e.,

$$\omega_3 = w_3 + \zeta_3. \tag{B6}$$

Since the vorticity vector $\boldsymbol{J}^\dagger$ (often referred to in the literature as the circulation) is a constant of motion for the nonviscous affine model (see CL85), we see from equations (B2) and (B6) that if initially the affine model has no internal motion, i.e., $\boldsymbol{J}^\dagger = 0$, then

$$\boldsymbol{w}(t) + \boldsymbol{\zeta}(t) = 0 \tag{B7}$$

at any time t.

REFERENCES

Aizenman, M. L. 1968, *Ap. J.*, **153**, 511.
Bicknell, G. V., and Gingold, R. A. 1983, *Ap. J.*, **273**, 749.
Carter, B., and Luminet, J. P. 1982, *Nature*, **296**, 211 (CL82).
______. 1983, *Astr. Ap.*, **121**, 97 (CL83).
______. 1985, *M.N.R.A.S.*, **212**, 23 (CL85).
Chandrasekhar, S. 1963, *Ap. J.*, **138**, 1182.
______. 1969, *Ellipsoidal Figures of Equilibrium* (New Haven: Yale University Press).
Cox, J. P., and Giuli, R. T. 1968, *Principles of Stellar Structure* (New York: Gordon & Breach).
Darwin, G. H. 1911, *The Tides* (3d ed.; London: John Murray), p. 340.
Frank, J. 1979, *M.N.R.A.S.*, **187**, 883.
Frank, J., and Rees, M. J. 1976, *M.N.R.A.S.*, **116**, 633.
Gradshteyn, I. S., and Ryzhik, I. M. 1980, *Tables of Integral Series and Products* (New York: Academic).
Gurzadyan, V. G., and Ozernoy, I. M. 1980, *Astr. Ap.*, **86**, 315.
Hills, J. G. 1975, *Nature*, **254**, 295.
______. 1978, *M.N.R.A.S.*, **182**, 517.
Luminet, J. P., and Marck, J. A. 1985, *M.N.R.A.S.*, **212**, 57.
Luminet, J. P., and Pichon, B. 1986, Observatoire de Meudon, preprint.
Michell, J. 1784, *Phil. Trans. Roy. Soc. London*, **74**, 35.
Nduka, A. 1971, *Ap. J.*, **170**, 131.
Nolthenius, R. A., and Katz, J. I. 1983, *Ap. J.*, **269**, 297.
Pichon, B. 1985, *Astr. Ap.*, **145**, 387.
______. 1986, Ph.D. thesis, Observatoire de Paris.
Roche, E. 1847–1850, *Mém. Acad. Sci. Montpellier*, **1**, 243–262, 333–348.
Wheeler, J. A. 1971, *Pontif. Acad. Sci. Scripta Vari*, **35**, 539.
Young, P. J., Shields, G. A., and Wheeler, J. C. 1977, *Ap. J.*, **212**, 367.

JEAN-PIERRE LUMINET and BRANDON CARTER: Groupe d'Astrophysique Relativiste, Observatoire de Paris, Section d'Astrophysique, 92195 Meudon Principal Cédex, France